Published for SISSA by Springer

Received: March 12, 2026
Revised: May 7, 2026
Accepted: May 22, 2026
Published: July 8, 2026

Improved branching-fraction measurements of $B^0_{(s)} \to K^0_S h^+ h'^-$ decays and first observation of $B^0_s \to K^0_S K^+ K^-$

The LHCb collaboration

Full author list at the end of the paper

E-mail: edoardo.mariani@cern.ch

Abstract: This paper presents a study of the charmless three-body decays $B^0_{(s)} \to K^0_S h^+ h'^-$ (where $h^{(\prime)} = \pi, K$), using a sample of pp collision data collected by the LHCb experiment during Runs 1 and 2 of the LHC, corresponding to an integrated luminosity of $9\,\text{fb}^{-1}$. The decay $B^0_s \to K^0_S K^+ K^-$ is observed for the first time, and the following ratios of branching fractions are measured:

$$\frac{\mathcal{B}(B^0 \to K^0_S K^+ K^-)}{\mathcal{B}(B^0 \to K^0_S \pi^+ \pi^-)} = 0.578 \pm 0.007 \pm 0.017\,,$$

$$\frac{\mathcal{B}(B^0 \to K^0_S K^\pm \pi^\mp)}{\mathcal{B}(B^0 \to K^0_S \pi^+ \pi^-)} = 0.1363 \pm 0.0035 \pm 0.0051\,,$$

$$\frac{\mathcal{B}(B^0_s \to K^0_S \pi^+ \pi^-)}{\mathcal{B}(B^0 \to K^0_S \pi^+ \pi^-)} = 0.269 \pm 0.011 \pm 0.015 \pm 0.008\,,$$

$$\frac{\mathcal{B}(B^0_s \to K^0_S K^+ K^-)}{\mathcal{B}(B^0 \to K^0_S \pi^+ \pi^-)} = 0.0303 \pm 0.0041 \pm 0.0025 \pm 0.0009\,,$$

$$\frac{\mathcal{B}(B^0_s \to K^0_S K^\pm \pi^\mp)}{\mathcal{B}(B^0 \to K^0_S \pi^+ \pi^-)} = 1.818 \pm 0.021 \pm 0.031 \pm 0.056\,,$$

where the uncertainties are statistical, systematic, and due to knowledge of the ratio of hadronisation fractions of the B^0_s and B^0 mesons, respectively.

Keywords: B Physics, Branching fraction, Flavour Physics, Hadron-Hadron Scattering

ArXiv ePrint: 2603.08621

This paper is dedicated to the memory of our friend and colleague Roger Barlow.

Open Access, Copyright CERN,
for the benefit of the LHCb Collaboration.
Article funded by SCOAP^3.

https://doi.org/10.1007/JHEP07(2026)071

JHEP07(2026)071

Contents

1 Introduction **1**

2 Detector and simulation **3**

3 Trigger and event selection **4**

4 Fit model **7**

5 Determination of the efficiencies **13**

6 Systematic uncertainties **15**
6.1 Fit model and yield measurement uncertainties 15
6.2 Efficiency uncertainties 16
6.3 Combination 17

7 Results and conclusion **18**

A Fits to all subsamples **20**

B Definition of the signal model **22**

C Correlation matrices **23**
C.1 Statistical correlation matrix 23
C.2 Correlation matrices due to the efficiency binning scheme 24

The LHCb collaboration **30**

1 Introduction

The charmless three-body decay processes of neutral B mesons, of the type $B^0_{(s)} \to K^0_S h^+ h'^-$ ($h^{(\prime)} = \pi, K$),[1] receive contributions from several Feynman-diagram topologies. In the Standard Model (SM), the decays $B^0 \to K^0_S \pi^+ \pi^-$ and $B^0 \to K^0_S K^+ K^-$ are particularly dominated by $b \to q\bar{q}s$ ($q = u, d, s$) loop transitions. New particles and interactions, foreseen in various SM extensions, may alter the amplitudes responsible for the decay process [1–3]. Thus, measuring the branching fractions and CP-violating asymmetries of these modes and comparing them with theoretical predictions is of great interest. As in other multibody hadronic decay modes of B hadrons, accurate theoretical predictions of branching fractions are challenging due to the presence of multiple interfering amplitudes. Precision measurements of branching fractions are therefore important inputs for further refining different theoretical approaches such as QCD factorisation or perturbative QCD [4–9], enabling better predictions of branching fractions and of CP asymmetries, both for the modes considered in this paper and for other charmless decay modes. These measurements also offer a means to evaluate

[1] Unless stated otherwise, charge-conjugate modes are implicitly included throughout this article.

JHEP07(2026)071

the degree of isospin, U-spin, and SU(3) flavour-symmetry breaking, as illustrated, for example, in ref. [10].

Studies of the decays of B^0 mesons to $K^0_S\pi^+\pi^-$, $K^0_S K^\pm\pi^\mp$, and $K^0_S K^+K^-$ final states were performed by the first-generation B-factory experiments, BaBar and Belle [11–15]. The first study of $B^0_{(s)}\to K^0_S h^+h'^-$ branching fractions performed by the LHCb collaboration, using the data sample recorded in 2011 corresponding to an integrated luminosity of $1\,\text{fb}^{-1}$ [16], reported the first observation of $B^0_s\to K^0_S\pi^+\pi^-$ and $B^0_s\to K^0_S K^\pm\pi^\mp$ decays, but found no evidence for the $B^0_s\to K^0_S K^+K^-$ decay. This study was subsequently updated with the full 2011–2012 data sample, corresponding to an integrated luminosity of $3.0\,\text{fb}^{-1}$ [17]; once again, no conclusive evidence for the decay $B^0_s\to K^0_S K^+K^-$ was found, with the significance of the corresponding signal found to be 2.5 standard deviations. The search reported here, using a much larger data sample, is therefore strongly motivated.

The selection criteria and mass fit procedures developed in this analysis for branching-fraction measurements may be reused in subsequent amplitude analyses, which provide access to more observables enabling detailed understanding of the decay dynamics. In such analyses, the contributing intermediate resonances can be disentangled, allowing the branching fractions and *CP*-violation parameters of the intermediate decay modes to be determined. The measurement of such *CP*-violation observables in $B^0_{(s)}\to K^0_S h^+h'^-$ decays is of significant theoretical interest. In particular, the mixing-induced *CP* asymmetries in the decays dominated by loop transitions, such as $B^0\to\phi K^0_S$, are predicted by the Cabibbo-Kobayashi-Maskawa (CKM) paradigm [18, 19] to differ only slightly from those of $b\to c\bar{c}s$ transitions, such as $B^0\to J/\psi K^0_S$. Within the SM, any deviations are expected to be small or may be controlled through flavour symmetries [20–22], whereas new particles and interactions could introduce additional weak phases, potentially leading to significantly larger deviations [1–3]. The mixing-induced *CP*-violating phase can be determined through a flavour-tagged, time-dependent amplitude analysis within the phase space of these three-body decay processes [13, 15, 23, 24]. The current experimental uncertainties [25, 26] remain substantially larger than the expected deviations, both within the SM and in scenarios extending beyond it, thereby motivating more precise measurements of these observables. Similarly, the mixing-induced *CP*-violating phase in the B^0_s system could be measured through $b\to q\bar{q}s$ processes such as $B^0_s\to K^0_S K^\pm\pi^\mp$ decays [27]. The CKM angle γ can also be determined by combining information obtained from several $B\to Khh'$ decays, including the branching fractions of these modes [28–30]. Experimental results from the BaBar collaboration [31, 32] demonstrate the feasibility of this measurement, albeit with large statistical uncertainties. Another method was suggested in refs. [33–35] and applied to amplitude models previously measured by BaBar [36], yielding several possible values of γ. The decay $B^0_s\to K^0_S\pi^+\pi^-$ is dominated by tree-level processes, and thus offers a potential theoretically cleaner determination of the angle γ [37].

In this paper, decays of B^0 and B^0_s mesons to the charmless three-body final states $K^0_S\pi^+\pi^-$, $K^0_S K^\pm\pi^\mp$, and $K^0_S K^+K^-$ are studied with the pp collision data recorded by the LHCb detector, corresponding to an integrated luminosity of $1.0\,\text{fb}^{-1}$ at a centre-of-mass energy of $\sqrt{s}=7\,\text{TeV}$ in 2011, $2.0\,\text{fb}^{-1}$ at $\sqrt{s}=8\,\text{TeV}$ in 2012, and $6\,\text{fb}^{-1}$ at $\sqrt{s}=13\,\text{TeV}$ from 2015 to 2018. The integrated luminosity is approximately three times larger than that used in ref. [17], which this paper supersedes. Furthermore, the production cross-

JHEP07(2026)071

section of B^0 and B_s^0 mesons increases with the centre-of-mass energy [38]. The time-integrated, *CP*-averaged branching fractions are measured relative to the $B^0 \to K_S^0\pi^+\pi^-$ decay. For B_s^0 decays, this implies that the contribution arising from nonzero width difference is included [39]. Throughout this document, the notation $\mathcal{B}(B^0 \to K_S^0 K^\pm\pi^\mp)$ refers to the sum of the branching fractions $\mathcal{B}(B^0 \to K_S^0 K^+\pi^-)$ and $\mathcal{B}(B^0 \to K_S^0 K^-\pi^+)$, and the same applies to the corresponding B_s^0 decays.

2 Detector and simulation

The LHCb detector [40, 41] is a single-arm forward spectrometer covering the pseudorapidity range $2 < \eta < 5$, designed for the study of particles containing b or c quarks. The detector used to collect the data analysed in this paper includes a high-precision tracking system consisting of a silicon-strip vertex detector surrounding the pp interaction region (the VELO), a large-area silicon-strip detector located upstream of a dipole magnet with a bending power of about 4 T m, and three stations of silicon-strip detectors and straw drift tubes placed downstream of the magnet. The tracking system provides a measurement of the momentum, p, of charged particles with a relative uncertainty that varies from 0.5% at low momentum to 1.0% at 200 GeV/c. The minimum distance of a track to a primary pp collision vertex (PV), the impact parameter (IP), is measured with a resolution of $(15 + 29/p_T)$ μm, where p_T is the component of the momentum transverse to the beam, in GeV/c. Different types of charged hadrons are distinguished using information from two ring-imaging Cherenkov detectors. Photons, electrons and hadrons are identified by a calorimeter system consisting of scintillating-pad and preshower detectors, an electromagnetic and a hadronic calorimeter. Muons are identified by a system composed of alternating layers of iron and multiwire proportional chambers.

Simulation is required to model the effects of the detector acceptance and selection requirements and to investigate backgrounds from other b-hadron decays. In the simulation, pp collisions are generated using Pythia [42, 43] with a specific LHCb configuration [44]. Decays of unstable particles are described by EvtGen [45], in which final-state radiation is generated using Photos [46]. The interaction of the generated particles with the detector, and its response, are implemented using the Geant4 toolkit [47, 48] as described in ref. [49].

To account for possible mismodelling of the detector response in simulation, in particular that of the particle identification (PID) systems, dedicated data and simulated calibration samples are used to correct the values of the corresponding variables for each candidate reconstructed in the simulated signal samples. The PID corrections are based on matching the cumulative distribution function (CDF) of the variable in question between the data and simulation calibration samples [50]. The variation of the PID response with the kinematics of the track and the occupancy of the detector is accounted for using a kernel density estimation in the four dimensions: PID variable CDF, p_T and η of the track, and the track multiplicity of the event [51].

JHEP07(2026)071

3 Trigger and event selection

The online event selection is performed by a trigger [52], which consists of a hardware stage, based on information from the calorimeter and muon systems, followed by a software stage, which applies a full event reconstruction. At the hardware trigger level, events are required to have a muon with high p_{T} or a hadron, photon or electron with high transverse energy in the calorimeters. For the decay modes considered, all of these triggers can be caused by activity in the event not associated with the signal candidate and, for the hadron triggers, they can also be caused by the signal candidate itself. The software trigger requires a two-, three- or four-track secondary vertex with a significant displacement from all primary pp interaction vertices. At least one charged particle must have high transverse momentum and be inconsistent with originating from any reconstructed PV. A multivariate algorithm [53, 54] is used for the identification of secondary vertices consistent with the decay of a b hadron. It is required that the software trigger decision must have been caused entirely by tracks from the decay of the signal B candidate.

To suppress background, events satisfying the trigger requirements are filtered in two subsequent stages: a set of loose preselection requirements, followed by an optimised multivariate selection. A potential source of systematic uncertainty is the accuracy of modelling the variation of the selection efficiency over the phase space of the B decay. To mitigate this, the selection is designed to minimise efficiency variations by imposing only loose requirements on properties (such as the momenta) of the individual B-meson decay products. Instead, extensive use is made of topological features such as the flight distance of the B candidate. The calculated values of these features depend on the assumption that the B candidate (or its decay products) have originated from a particular PV. To remove ambiguity, it is therefore necessary to associate each candidate with a single PV, that from which it is most consistent with having originated. The metric for defining the consistency is the χ^2_{IP} quantity, which is the difference in vertex-fit χ^2 of the given PV reconstructed with and without the candidate in question. In events that contain more than one PV, each candidate is associated with the PV with which it forms the smallest χ^2_{IP} value.

Candidate $K^0_{\mathrm{S}} \to \pi^+\pi^-$ decays are reconstructed in two different categories: the first involving K^0_{S} mesons that decay early enough for the resulting pions to be reconstructed in the VELO; and the second contains those K^0_{S} mesons that decay further downstream, such that track segments of the pions cannot be formed in the VELO. These K^0_{S} reconstruction categories are referred to as *long* (LL) and *downstream* (DD), respectively. The long category has better mass, momentum and vertex resolution than the downstream category. There are, however, approximately twice as many K^0_{S} candidates reconstructed as DD than as LL, due to the lifetime of the K^0_{S} meson and the geometry of the detector. In the following, B candidates whose decay products include either a long or downstream K^0_{S} candidate are referred to using the corresponding category names. During the 2012 data taking, a significant improvement of the trigger efficiency for downstream K^0_{S} candidates was obtained following an update of the software trigger algorithms. To take this into account, the 2012 data sample is subdivided into the 2012a and 2012b data-taking periods.

The K^0_{S} candidates are formed by combining two oppositely charged pions, both of which are required to have momentum $p > 2\,\mathrm{GeV}/c$ and have χ^2_{IP} with respect to their associated

JHEP07(2026)071

PV greater than 9 (4) for long (downstream) candidates. The vertex of the K^0_S candidate is determined and the resulting mass must be within $\pm 20\,\text{MeV}/c^2$ ($\pm 30\,\text{MeV}/c^2$) of the known K^0_S mass [26] for long (downstream) candidates. To discriminate against tracks originating from the PV, the K^0_S vertex is required to be significantly displaced from its associated PV, as quantified by χ^2_{VS}, the difference in vertex-fit χ^2 when the secondary vertex is constrained to coincide with the primary vertex. In addition, downstream K^0_S candidates are required to have a momentum $p > 6\,\text{GeV}/c$.

The B candidates are formed by combining a K^0_S candidate and two oppositely charged particles, $h^+h'^-$, initially assuming the pion-mass hypothesis. The momenta of both charged particles are required to be in the range $3 < p < 100\,\text{GeV}/c$ to ensure good pion-kaon discrimination. Both charged particles should also be inconsistent with being muons based on information from the muon system. The scalar sum of the transverse momenta of the K^0_S, h^+, and h'^- candidates must be greater than $3.0\,\text{GeV}/c$ ($4.2\,\text{GeV}/c$), for long (downstream) candidates, and at least two of the three decay products must have $p_{\text{T}} > 0.8\,\text{GeV}/c$. The B candidates must have $p_{\text{T}} > 1.5\,\text{GeV}/c$ and mass within the range $4000 < m_{K^0_S\pi^+\pi^-} < 6200\,\text{MeV}/c^2$. The fitted B-candidate decay vertex should be significantly separated from any PV, and isolated from other tracks, as quantified by the change in vertex-fit chi-square, χ^2_{vtx}, when adding any other track in the event. The B candidates should also be consistent with originating from a PV, quantified by requiring, for long (downstream) candidates, both that $\chi^2_{\text{IP}} < 8\,(6)$ and that the cosine of the angle θ_{DIR} between the reconstructed momentum vector of the B candidate and the vector between the associated PV and the decay vertex be greater than 0.9999 (0.999). Finally, the decay vertex of the K^0_S candidate is required to be at least 30 mm downstream, along the beam direction, from that of the B candidate. In conjunction with the K^0_S mass requirement, this suppresses direct four-body decays $B^0_{(s)} \to h^+h'^-\pi^+\pi^-$, as well as misreconstructed $B^0_{(s)} \to K^0_S h^+h'^-$ decays in which a pion produced in the K^0_S decay is exchanged with the h or h' track of the same charge.

The next stage of the selection uses dedicated multivariate discriminants trained using the XGBoost implementation [55] of a boosted decision tree (BDT) algorithm [56]. Two different types of classifiers are trained, each designed to suppress a particular background contribution. The first is designed to suppress the combinatorial background and mainly uses information on the decay topology. Since the different signal channels have almost identical topologies, the same BDT is used for all channels. In contrast, the second classifier, referred to as the PID BDT in the following, is designed to suppress background from so-called cross-feed backgrounds, where a signal decay from one signal channel is misidentified as being from another signal channel, *e.g.* a $B^0_s \to K^0_S K^\pm\pi^\mp$ decay where the final-state kaon is misidentified as a pion and so is reconstructed as a candidate in the $K^0_S\pi^+\pi^-$ spectrum. Accordingly, this latter classifier is trained using information from the particle-identification systems and separate classifiers are trained for each of the signal final states.

The features used in the topological BDT training are: the p_{T}, η, χ^2_{IP}, χ^2_{VS}, $\cos\theta_{\text{DIR}}$ and χ^2_{vtx} values of the B candidate; the smallest change in the B-candidate χ^2_{vtx} value when adding another track from the event; the sum of the χ^2_{IP} values of the h^+ and h'^- candidates and, in the case of the long category, additionally that of the K^0_S candidate; and the χ^2_{VS} of the K^0_S candidate for the long category only. Additional variables included are

JHEP07(2026)071

four asymmetries of the form

$$X^{\text{asym}} \equiv \frac{X^P - X^{\text{cone}}}{X^P + X^{\text{cone}}}\,, \tag{3.1}$$

where X^P is the quantity X (p or p_{T}) for particle P (B or K^0_{S}) and X^{cone} is the same quantity determined from a vector sum of the momenta of all charged tracks inside a cone around the direction of particle P, of radius $R \equiv \sqrt{\delta\eta^2 + \delta\phi^2} = 1.5$. Here $\delta\eta$ and $\delta\phi$ are the difference in pseudorapidity and azimuthal angle (in radians) around the beam direction, between the momentum vector of the track under consideration and that of particle P. Finally, four differences of the form

$$Y^{\text{diff}} \equiv Y^P - Y^{\text{cone}}\,, \tag{3.2}$$

where the quantity Y is either η or ϕ, are also included in the BDT. The signal and background training samples are, respectively, simulated $B^0 \to K^0_{\text{S}}\pi^+\pi^-$ decays and data from the upper mass sideband, $5425 < m_{K^0_{\text{S}}\pi^+\pi^-} < 6200\,\text{MeV}/c^2$. Contributions from $\Lambda_b^0 \to \Lambda_c^+ h^-$, $\Lambda_c^+ \to K^0_{\text{S}} p$ decays are removed from the training samples taken from data, using mass vetoes.

The features used to train the PID BDT are the outputs of multivariate classifiers applied to the h^+ and h'^- candidates, each designed to identify kaons, pions, and protons using information from the particle-identification and tracking detectors. The PID BDT for a given final state is trained using simulation, where the signal training sample consists of decays of the channel in question, while the background training sample contains different $B^0_{(s)} \to K^0_{\text{S}} h^+ h'^-$ decay modes. For both signal and background training samples, the candidates are reconstructed under the mass hypothesis of the final state being considered, meaning that in the background sample one of the final-state hadrons has been assigned the wrong identity.

The selection requirements placed on the output of the two BDTs are simultaneously optimised. The optimisation is performed independently for each data-taking year, with 2012 subdivided as mentioned above, and for each K^0_{S} reconstruction type. It is also performed separately for the B^0 and B^0_s signals that are present in each final state, since the expected yields of the two decays can differ greatly. The selection optimisation for those modes that are favoured ($B^0 \to K^0_{\text{S}}\pi^+\pi^-$, $B^0_s \to K^0_{\text{S}}K^\pm\pi^\mp$, $B^0 \to K^0_{\text{S}}K^+K^-$) is referred to as looser, and the selection optimisation for those modes that are suppressed ($B^0_s \to K^0_{\text{S}}\pi^+\pi^-$, $B^0 \to K^0_{\text{S}}K^\pm\pi^\mp$, $B^0_s \to K^0_{\text{S}}K^+K^-$) is referred to as tighter. For all signal decay modes that have previously been observed, the following figure of merit is used

$$\mathcal{Q}_1 \equiv \frac{N_{\text{sig}}}{\sqrt{N_{\text{sig}} + N_{\text{bg}}}}\,, \tag{3.3}$$

where N_{sig} (N_{bg}) represents the number of expected signal (combinatorial background) candidates that are retained by a given selection and fall within the signal region. The signal region is defined as a mass window of ± 2.5 times the estimated signal resolution around the known B^0 or B^0_s mass [26], as appropriate. The value of N_{sig} is estimated based on the known branching fractions [26] and the signal efficiency (ε_{sig}) determined from simulation. Due to the simultaneous optimisation of the two BDTs, the calculation of N_{bg} must include both combinatorial and cross-feed background sources. The expected

JHEP07(2026)071

number of cross-feed candidates is calculated similarly to $N_{\rm sig}$, while the number of expected combinatorial candidates is determined by fitting the mass distribution above the signal region ($5550 < m_{K^0_S h^+ h'^-} < 6200\,\text{MeV}/c^2$) and extrapolating into the signal region. The $B^0_s \to K^0_S K^+ K^-$ mode is yet to be observed and so an alternative figure of merit is used that does not require knowledge of the signal branching fraction [57],

$$\mathcal{Q}_2 \equiv \frac{\varepsilon_{\rm sig}}{\frac{5}{2} + \sqrt{N_{\rm bg}}}\,, \tag{3.4}$$

where the value of $N_{\rm bg}$ is estimated in the same way as described for $\mathcal{Q}_1$.

A final category of background that must be considered consists of fully reconstructed b-hadron decays into a $K^0_S h^+ h'^-$ final state that proceed via an intermediate charm or charmonium state, *e.g.* two-body Dh, $\Lambda_c^+ h$ or $(c\bar{c})K^0_S$ combinations, where $(c\bar{c})$ indicates a charmonium resonance. Such decays often satisfy the selection criteria with reasonably high efficiency and may result in a very similar B-candidate mass distribution as the signal candidates. Therefore, the following decays are explicitly reconstructed under the relevant particle mass hypotheses and vetoed in all the spectra: $D^0 \to K^-\pi^+$, $D^+ \to K^0_S K^+$, $D^+ \to K^0_S \pi^+$, $D^+_s \to K^0_S K^+$, $D^+_s \to K^0_S \pi^+$, $\Lambda_c^+ \to p K^0_S$, $J/\psi \to \pi^+\pi^-$, $J/\psi \to K^+K^-$, $\chi_{c0} \to \pi^+\pi^-$, and $\chi_{c0} \to K^+K^-$. The vetoed mass region for each reconstructed charm (charmonium) state is a window of $\pm 30\,(\pm 48)\,\text{MeV}/c^2$ around the known mass of that state [26]. This range reflects the typical mass resolution obtained at LHCb. Similarly, backgrounds from $\Lambda \to p\pi^-$ decays being reconstructed as $K^0_S \to \pi^+\pi^-$ are suppressed by applying a mass veto window of $\pm 6.8\,\text{MeV}/c^2$ around the known Λ mass [26] when applying the $p\pi^-$ or $\pi^+\bar{p}$ mass hypothesis to the K^0_S-candidate decay products.

4 Fit model

The data are divided into seven statistically independent subsamples, separated by data-taking period (2011, 2012a, 2012b, 2015, 2016, 2017, 2018). The selected B candidates form eight mass spectra: four final states ($K^0_S\pi^+\pi^-$, $K^0_S K^+\pi^-$, $K^0_S\pi^+K^-$, $K^0_S K^+K^-$) multiplied by two K^0_S reconstruction types (LL, DD). For each subsample, simultaneous unbinned maximum-likelihood fits to the eight mass spectra in the range 5100–5750 MeV/c^2 are used to determine the signal yields. In general, each final state will contain two signal peaks, B^0 and B^0_s, and, as discussed above, the optimum working point in the selection is significantly different between the two peaks (referred to as the tighter and looser selections for the suppressed and favoured decay modes, respectively). To minimise the expected statistical uncertainties on the ratios of branching fractions, the fit procedure described below is performed twice for each subsample: once with the tighter selections, to be used to measure the branching fractions of the $B^0 \to K^0_S K^\pm \pi^\mp$, $B^0_s \to K^0_S \pi^+\pi^-$, and $B^0_s \to K^0_S K^+K^-$ decays relative to that of the $B^0 \to K^0_S \pi^+\pi^-$ decay; and once with the looser selections, to be used to measure the branching fractions of the $B^0 \to K^0_S K^+K^-$ and $B^0_s \to K^0_S K^\pm\pi^\mp$ decays relative to that of the $B^0 \to K^0_S\pi^+\pi^-$ decay.

Several different components contribute to each mass spectrum. Those considered in the baseline fit model are the two signal peaks arising from correctly reconstructed B^0 and B^0_s signal decays, cross-feed structures due to other $B^0_{(s)} \to K^0_S h^+ h'^-$ decays in which one or both

JHEP07(2026)071

charged hadrons is misidentified, partially reconstructed decays of a b hadron to a final state of the form $K^0_S h^+ h'^- X$ where the system X is not reconstructed, and combinatorial background.

Each signal peak is modelled as the sum of two Crystal Ball functions [58], which share common peak position (μ) and width (σ) parameters, but whose power-law tails are on opposite sides of the peak and have separate parameters (n_L, n_R, α_L, α_R). An additional parameter (f_L) determines the fraction of candidates in the left-tailed Crystal Ball function, for a total of seven shape parameters. A simultaneous fit to the eight mass spectra in simulated signal events of the subsample under consideration is used to determine the lineshape parameters, with certain parameters (or ratios of parameters) shared between mass spectra and between the B^0 and B^0_s peaks; see appendix B for details. In particular, the peak position parameters $\mu(B^0)$ and $\mu(B^0_s)$ are common across all spectra, and the width parameters σ are defined relative to one reference peak, corresponding to the $B^0 \to K^0_S \pi^+ \pi^-$ decay with downstream K^0_S reconstruction. When fitting to a subsample of data, only two of the signal shape parameters are free to vary, with all others being derived from those two or fully fixed from the fit to simulated data. The two free shape parameters are the B^0 peak position parameter, with the B^0_s peak position derived according to $\mu(B^0_s) = \mu(B^0) + \Delta m$, where $\Delta m = 87.26\,\text{MeV}/c^2$ is the known difference in mass between the two states [26]; and the peak width parameter $\sigma(B^0 \to K^0_S \pi^+ \pi^-; \text{DD})$, with all other width parameters derived from it according to the ratios seen in the fit to simulation. It has been determined that the ratio of the widths in the downstream and long K^0_S reconstruction types of the $B^0 \to K^0_S \pi^+ \pi^-$ channel is well reproduced in the simulation. All signal yields are free to vary in the fit to data.

Cross-feed components occur due to hadron misidentification of the h^+ or h'^- mesons, such that events from one of the eight signal decay modes appear in a different mass spectrum, *e.g.* $B^0 \to K^0_S \pi^+ \pi^-$ decays may appear in the $K^0_S K^+ \pi^-$ spectrum if the π^+ is misidentified as a K^+. The probability for a misidentified decay to pass the selection is determined with simulation, corrected for known data-simulation differences, in the same way as the efficiency for a correctly identified decay to pass the selection, as described in section 6. Cross-feed components are modelled similarly to the signal, using the sum of two Crystal Ball functions. For each combination of a true decay and reconstructed final state, the shape parameters are determined from a fit to simulated signal events of the true decay that pass the selection for the reconstructed final state. This fit is performed simultaneously to all data-taking periods and to both K^0_S reconstruction types, and with the final states $K^0_S K^+ \pi^-$ and $K^0_S \pi^+ K^-$ combined. Double misidentification (*e.g.* $B^0 \to K^0_S \pi^+ \pi^-$ decays identified as $K^0_S K^+ K^-$) is found to be negligible, as is cross-feed from the suppressed decays $B^0_s \to K^0_S \pi^+ \pi^-$ and $B^0_s \to K^0_S K^+ K^-$. This leaves two cross-feed structures in each final state: $B^0 \to K^0_S K^\pm \pi^\mp$ and $B^0_s \to K^0_S K^\pm \pi^\mp$ in $K^0_S \pi^+ \pi^-$; $B^0 \to K^0_S \pi^+ \pi^-$ and $B^0 \to K^0_S K^+ K^-$ in $K^0_S K^\pm \pi^\mp$; and $B^0 \to K^0_S K^\pm \pi^\mp$ and $B^0_s \to K^0_S K^\pm \pi^\mp$ in $K^0_S K^+ K^-$. When fitting to a subsample of data, the shape of each cross-feed component is fixed from the fit to simulated data. Since the misidentification probabilities are known from simulation within some uncertainty, the yield of each misidentified cross-feed contribution may be appropriately constrained from this information and the yield of the corresponding correctly identified signal component with the same K^0_S reconstruction. For each final state, this is implemented by constraining the ratio of the yields of the two cross-feed structures; this leaves one free cross-feed yield-normalisation

JHEP07(2026)071

parameter per final state. In addition, when applying the tighter selection, a second constraint is added, such that the cross-feed yields are fully determined by the correctly identified signal yields and the misidentification probabilities. The uncertainty arising from the precision and accuracy of the misidentification probabilities derived from simulation is propagated as part of the systematic uncertainties.

A range of different physical processes contribute to partially reconstructed components; in each case, one or more final-state particles from the true decay are omitted in the reconstruction (*e.g.* $B^0 \to K^{*0}\pi^+\pi^-$, $K^{*0} \to K^0_S\pi^0$ with the π^0 omitted). Because part of the four-momentum is missing in such decays, the lineshape is, in general, displaced to lower mass. Since the fit range starts at $5100\,\text{MeV}/c^2$, a complete description of all partially reconstructed decays is not required: often, the bulk of their distribution lies below the lower fit boundary. Instead, simulated samples of a small number of decay modes are used, and in each case the lineshape is modelled as the convolution of a generalised ARGUS function [59] with a Gaussian function, using a simultaneous fit to all data-taking periods and to both K^0_S reconstruction types. For partially reconstructed charmless decays, the representative decay mode used is $B^0 \to K^*(892)^0\rho(770)^0$, with $K^*(892)^0 \to K^0_S\pi^0$ and $\rho(770)^0 \to \pi^+\pi^-$ with the π^0 omitted, and the lineshape obtained is used for all final states and for both partially reconstructed $B_{d/u}$ and B^0_s decays (with an offset of $+\Delta m$ when the source is a B^0_s decay). When fitting to a subsample of data, the shape of each partially reconstructed component is fixed from the fits to simulated data. Each final state contains two charmless partially reconstructed components ($B_{d/u}$ and B^0_s), and their yields are free to vary in the fit to data. Other contributions are considered as systematic variations, as described in section 6.1.

The combinatorial background component, arising from unrelated or uncorrelated combinations of final-state particles, is parameterised as a first-order polynomial function. When fitting to a subsample of data, the yield and slope of the combinatorial component are free to vary for each final state, except that the $K^0_S K^+\pi^-$ and $K^0_S\pi^+K^-$ final states share a common slope parameter.

The individual fits to the subsamples can be found in appendix A. For illustration, the sum of all of the individual fits are shown, together with the combined dataset, in figure 1 for the tighter selection, and in figure 2 for the looser selection. The total fitted signal yields, summed across all subsamples, are given in table 1 with statistical uncertainties only. In addition to the signal yields, the fit output is also used to compute signal weights via the *sPlot* method [60, 61]; these are used for certain data-simulation corrections as described below. They are also used to construct the signal Dalitz plots for each decay that are shown in figure 3. The total yield of $B^0_s \to K^0_S K^+K^-$, combining the long and downstream K^0_S reconstruction types, is found to be 207 ± 21 with the tighter selection, for which the corresponding significance, based on the ratio of yield to statistical uncertainty, is approximately 10 standard deviations.

JHEP07(2026)071

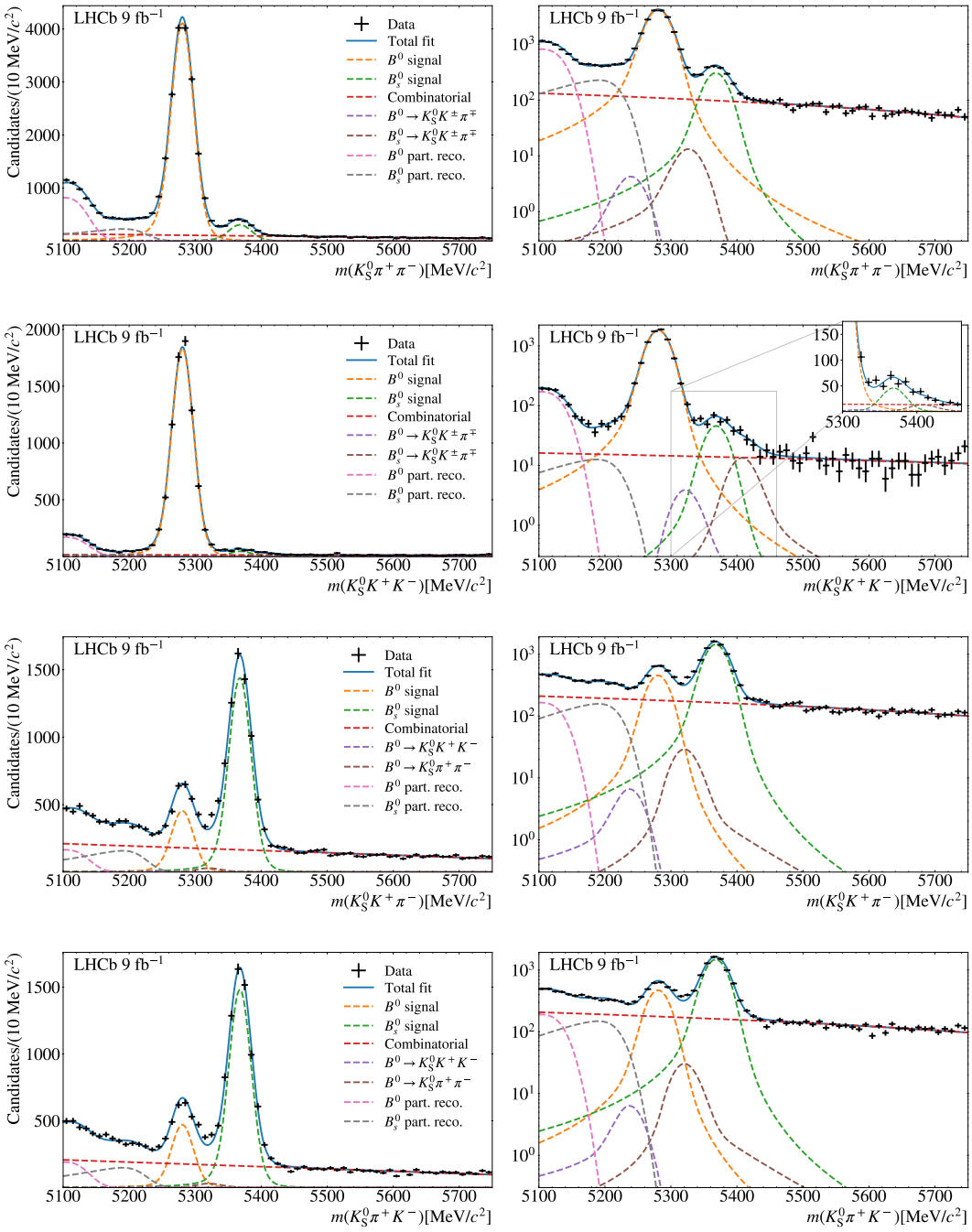

Figure 1. Mass distributions of $K_S^0 h^+ h'^-$ candidates that pass the tighter selection, combining all running periods and both K_S^0 reconstruction types. The tighter selection is used to measure the ratios of branching fractions with the following decays in the numerator: $B_s^0 \to K_S^0 \pi^+ \pi^-$, $B^0 \to K_S^0 K^\pm \pi^\mp$, $B_s^0 \to K_S^0 K^+ K^-$. For illustration, the sum of the fits to the subsamples is also shown. From top to bottom, each row corresponds to a different final state: $K_S^0 \pi^+ \pi^-$, $K_S^0 K^+ K^-$, $K_S^0 K^+ \pi^-$, $K_S^0 \pi^+ K^-$. The inset zooms into the $B_s^0 \to K_S^0 K^+ K^-$ signal region.

JHEP07(2026)071

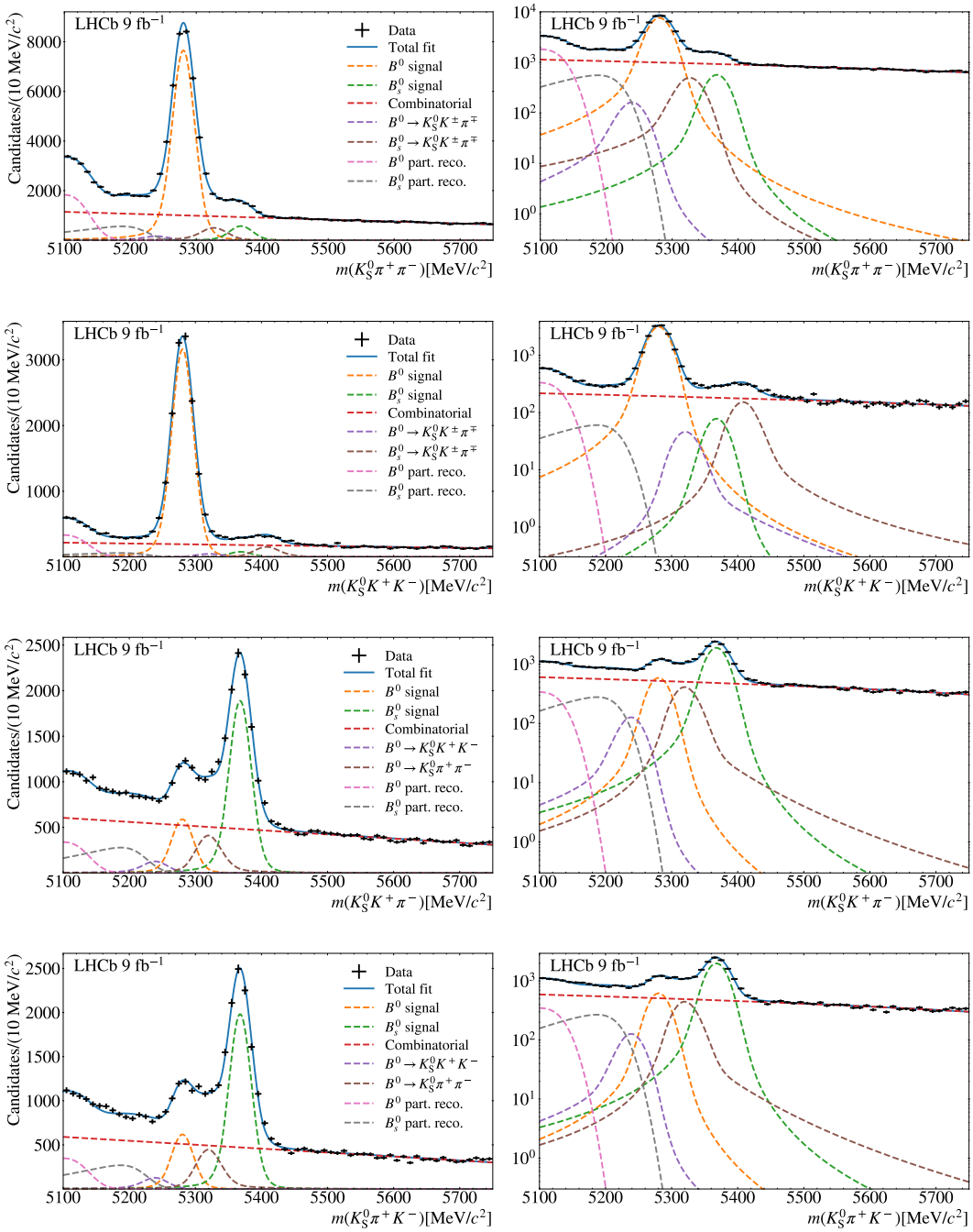

Figure 2. Mass distributions of $K_S^0 h^+ h'^-$ candidates that pass the looser selection, combining all running periods and both K_S^0 reconstruction types. The looser selection is used to measure the ratios of branching fractions with the following decays in the numerator: $B_s^0 \to K_S^0 K^\pm \pi^\mp$, $B^0 \to K_S^0 K^+ K^-$. For illustration, the sum of the fits to the subsamples is also shown. From top to bottom, each row corresponds to a different final state: $K_S^0\pi^+\pi^-$, $K_S^0 K^+ K^-$, $K_S^0 K^+\pi^-$, $K_S^0\pi^+ K^-$.

JHEP07(2026)071

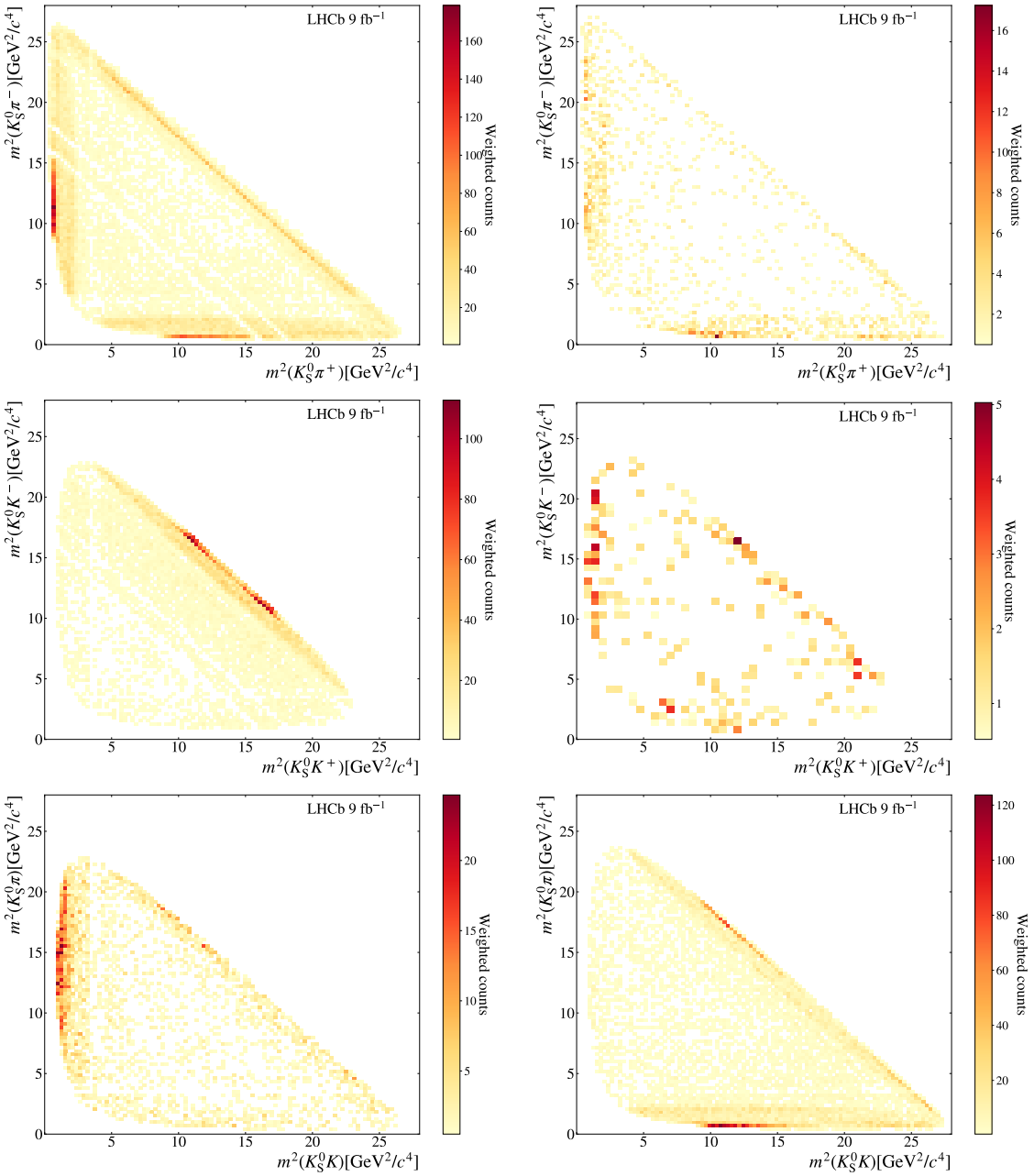

Figure 3. Signal Dalitz plots obtained using the signal weights computed from the results of the mass fits. From top to bottom, each row corresponds to (left) B^0 and (right) B^0_s decays to a final state: $K^0_S\pi^+\pi^-$, $K^0_SK^+K^-$, $K^0_SK^\pm\pi^\mp$. Bins with small negative entries are set to zero.

JHEP07(2026)071

Decay	Yield (looser)	Yield (tighter)
$B^0 \to K^0_S(\mathrm{LL})\pi^+\pi^-$	10930 ± 140	6920 ± 90
$B^0 \to K^0_S(\mathrm{DD})\pi^+\pi^-$	25040 ± 230	12360 ± 120
$B^0 \to K^0_S(\mathrm{LL})K^+K^-$	4280 ± 70	
$B^0 \to K^0_S(\mathrm{DD})K^+K^-$	9640 ± 120	
$B^0 \to K^0_S(\mathrm{LL})\pi^+K^-$		700 ± 40
$B^0 \to K^0_S(\mathrm{DD})\pi^+K^-$		1430 ± 60
$B^0 \to K^0_S(\mathrm{LL})K^+\pi^-$		576 ± 35
$B^0 \to K^0_S(\mathrm{DD})K^+\pi^-$		1480 ± 60
$B^0_s \to K^0_S(\mathrm{LL})\pi^+\pi^-$		485 ± 34
$B^0_s \to K^0_S(\mathrm{DD})\pi^+\pi^-$		980 ± 50
$B^0_s \to K^0_S(\mathrm{LL})K^+K^-$		60 ± 12
$B^0_s \to K^0_S(\mathrm{DD})K^+K^-$		147 ± 17
$B^0_s \to K^0_S(\mathrm{LL})\pi^+K^-$	2750 ± 70	
$B^0_s \to K^0_S(\mathrm{DD})\pi^+K^-$	6300 ± 110	
$B^0_s \to K^0_S(\mathrm{LL})K^+\pi^-$	2550 ± 70	
$B^0_s \to K^0_S(\mathrm{DD})K^+\pi^-$	6080 ± 110	

Table 1. Signal yields and the associated statistical uncertainties for each final state in data, combining results from fits to the seven data-taking periods, obtained at the two different selection working points (looser, tighter). Yields are quoted separately for the two K^0_S reconstruction types (LL, DD).

5 Determination of the efficiencies

The following expression is used to determine branching fractions of the $B^0_{(s)} \to K^0_S h^+ h'^-$ decays relative to the normalisation mode $B^0 \to K^0_S \pi^+ \pi^-$,

$$\frac{\mathcal{B}(B^0_{(s)} \to K^0_S h^+ h'^-)}{\mathcal{B}(B^0 \to K^0_S \pi^+ \pi^-)} = \frac{\varepsilon^{\mathrm{sel}}_{B^0 \to K^0_S \pi^+ \pi^-}}{\varepsilon^{\mathrm{sel}}_{B^0_{(s)} \to K^0_S h^+ h'^-}} \frac{N_{B^0_{(s)} \to K^0_S h^+ h'^-}}{N_{B^0 \to K^0_S \pi^+ \pi^-}} \frac{f_d}{f_{d(s)}}, \tag{5.1}$$

where $\varepsilon^{\mathrm{sel}}_X$ denotes the average efficiency of the decay mode X, N_X is the fitted signal yield, and f_d and f_s are the hadronisation fractions of a b quark into a B^0 or B^0_s meson, respectively. The efficiency term includes the geometrical acceptance and the trigger, reconstruction, and selection requirements. The ratio f_s/f_d has been measured previously at the LHCb experiment using hadronic and semileptonic decays at different centre-of-mass energies [62]. When calculating the branching fraction for a given data subsample, the value of f_s/f_d used is that corresponding to the centre-of-mass energy at which the subsample was recorded. The uncertainty on f_s/f_d is treated as being fully correlated across all subsamples.

Three-body hadronic decays such as $B^0_{(s)} \to K^0_S h^+ h'^-$ may proceed through quasi-two-body intermediate resonances, and may also include broad amplitudes, referred to as nonresonant, that may overlap and interfere with one another. The resulting distribution of events

JHEP07(2026)071

within the phase space is characterised as a Dalitz plot [63]. In the case of charmless three-body b-meson decays, the distribution is far from uniform, typically with much higher probability density near the boundaries of the Dalitz plot (as illustrated for the decay $B_s^0 \to K_S^0 K^\pm \pi^\mp$ in ref. [64]). Because the trigger, reconstruction, and selection efficiencies can vary considerably across the Dalitz plot, the efficiency $\varepsilon_X^{\text{sel}}$ is obtained by a weighted average across the phase space, with weights computed from the signal distribution. The signal distributions are determined from the data sample analysed: although for certain decay modes there are prior measurements of the Dalitz-plot distribution, these are drawn from smaller signal yields.

To simplify the description of the phase space, a transformation into a square Dalitz plot [65] is used; this has the benefit of spreading out the regions close to the kinematic boundaries where resonances are concentrated and where the efficiency varies rapidly. The square Dalitz plot is divided into bins in a 10×10 grid. For a data-taking period k, the efficiency within bin j is denoted $\varepsilon_{j,k}$ and is computed from simulated events, corrected for known data-simulation differences as described below.

For each subsample k of data, the fits to the $K_S^0 h^+ h'^-$ mass spectra described in section 4 are used to generate weights, $W_{j,k}$, using the *sPlot* technique [61], taking the $K_S^0 h^+ h'^-$ mass as the discriminating variable; these weights are then used to isolate the B^0 and B_s^0 signals in data and determine their distributions in the square Dalitz plots. Correlations between the Dalitz-plot variables and the discriminating variable are found to be sufficiently small to be neglected. While this can be done for all subsamples, the distributions are best determined with larger sample sizes. Therefore, for the purposes of averaging the efficiency, only the last three years $k' = \{2016, 2017, 2018\}$ are used (with distributions quantified as the sum of the weights $W_{j,k'}$ in each square Dalitz bin j), with a given subsample only included if the statistical significance of the signal yield exceeds 2 standard deviations. The only case where this requirement results in a subsample being excluded is in the determination of the $B_s^0 \to K_S^0 K^+ K^-$ distribution, where the 2016 LL subsample has an insignificant signal yield (1.5 ± 2.6). Each of these distributions is then corrected for efficiency in bins of the square Dalitz plot; the resulting efficiency-corrected, background-subtracted distribution may then be used to compute the average efficiency for any subsample, including those with smaller yields. The estimate of the weighted-average efficiency for subsample k, determined using the distribution of subsample k', is given by

$$\bar{\varepsilon}_{k,k'} = \frac{\sum_j W_{j,k'}\, \varepsilon_{j,k'}^{-1}\, \varepsilon_{j,k}}{\sum_j W_{j,k'}\, \varepsilon_{j,k'}^{-1}}. \tag{5.2}$$

Note that for each data-taking period k, there are three independent estimates of the average efficiency, one for each of the reference data-taking periods. These three estimates are then combined, taking the arithmetic mean without weighting (since the three reference data samples are approximately equal in size), to give single efficiency $\bar{\varepsilon}_k$ for each dataset k.

Known differences between data and simulation are corrected with calibration samples. For the h^+ and h'^- hadrons, differences in tracking efficiency are corrected as a function of the track momentum and pseudorapidity [66]. An analogous correction is applied to the K_S^0 tracking and vertex-reconstruction efficiency. Differences in hardware-trigger response between data and simulation are determined from samples of $D^{*+} \to D^0(\to K^-\pi^+)\pi^+$

JHEP07(2026)071

decays triggered by other activity in the event, and are determined as a function of the hadron charge, p_{T}, calorimeter region, and the overlap between the calorimeter clusters of the final-state particles in signal decays, including a correction for the average underlying energy in the calorimeter. Differences in particle-identification efficiency and misidentification rates between kaons and pions are determined from the same D^{*+} calibration samples; as noted in section 3, these corrections are applied before simulated decays are processed by the PID BDT. The tracking-efficiency corrections are of $\mathcal{O}(1\%)$, while those related to the trigger efficiency can be up to 10%.

The selection efficiency depends upon the b-hadron decay-time distribution. In the case of B_s^0 decays, the lifetime difference between the two CP eigenstates is significant, and at present the CP content of the three B_s^0 decays is unknown. The B_s^0 decay model used in the simulation assumes an effective lifetime of $1/\Gamma_s$, where Γ_s is the average width of the two CP-eigenstates of the B_s^0 meson. The relative change in the CP-averaged B_s^0 efficiency corresponding to a variation of the effective B_s^0 meson decay width of $\pm\Delta\Gamma_s/2$ is estimated to be $\mp 4\%$.

6 Systematic uncertainties

The branching fractions are measured relative to that of the decay $B^0 \to K^0_{\mathrm{S}}\pi^+\pi^-$, as shown in eq. (5.1). Similar selections and fit procedures are used for the numerator and denominator, and as a result, many systematic effects cancel at first order in the ratio. The remaining uncertainties are discussed below, grouped according to whether they influence the yield measurements (N) or the efficiency (ε); the uncertainty on f_s/f_d is treated separately. In most cases, systematic uncertainties are first evaluated on the individual measurements (split by data-taking period and K^0_{S} reconstruction type); the procedure by which these individual measurements are combined, and the systematic uncertainties on this combination, are discussed in section 6.3.

6.1 Fit model and yield measurement uncertainties

Several assumptions are made during the fit procedure, principally the models chosen to describe different components and the choices made when constraining or fixing fit parameters. For each of the 13 assumptions discussed below, the associated systematic uncertainty is evaluated by making a different assumption with respect to the baseline model and rerunning the full analysis up to the determination of the ratios of branching fractions (eq. (5.1)). The uncertainty on a given ratio for a given subsample is taken to be the absolute value of the difference between the result obtained with the baseline method and with the modified method. This is done separately for each ratio of branching fractions (with $B^0_{(s)} \to K^0_{\mathrm{S}}K^\pm\pi^\mp$ split by charge), each data-taking period, each K^0_{S} reconstruction type, and for the looser and tighter selections (*i.e.* for $7 \times 7 \times 2 \times 2$ configurations).

For the signal component, systematic uncertainties are assigned based on the two following modifications: replacing the signal model with a double-sided Hypatia function [67], or allowing the mass difference Δm between the B^0 and B_s^0 peaks to vary in the fit.

For the cross-feed component, the two following modifications are considered: the constraint on the ratio of yields of the two cross-feed peaks in each spectrum is removed, allowing

JHEP07(2026)071

them to vary independently; or the yields of cross-feed peaks are allowed to vary instead of being fully constrained when using the tighter selection.

For the partially reconstructed component, fits to representative simulated samples are used to determine the lineshape. In the baseline fit, the charmless decay $B^0 \to K^*(892)^0\rho(770)^0$ is used for B^0 and, with an offset, for B_s^0 decays. In the modified versions, a lineshape derived from fits to a sample of the hadronic decay $B^+ \to D^0\pi^+$, with $D^0 \to K^0_S\pi^+\pi^-$, is considered, first in place of the charmless decay, or second in addition to it. In a third variation, additional components are added to the $K^0_S\pi^+\pi^-$ spectrum to describe radiative decays.

For the combinatorial component, four variations are considered: the slope parameters for the final states $K^0_S K^+\pi^-$ and $K^0_S\pi^+K^-$ are allowed to differ, the slope parameter is allowed to take positive values, the slope parameter is fixed entirely according to a prior fit to the upper mass sideband 5500–5750 MeV/c^2, or the combinatorial model is replaced with an exponential function.

Finally, in the baseline fit procedure, very small components are suppressed because yields close to the lower bound of zero can cause fit instability: when the fit finds a component yield to be less than one event for a subsample, this is taken to be negligible and fixed to zero, and the data are refitted without that component. This procedure is instead modified in two ways: by fixing the yield to the fitted value, or by leaving the yield free.

For each subsample and configuration, the procedure above gives a set of 13 fit systematic uncertainties on each ratio of branching fractions. These 13 uncertainties are then combined in quadrature to give an uncertainty on each ratio of branching fractions for the subsample and configuration. These fit uncertainties on the individual subsamples are subsequently propagated, assuming no correlation among the subsamples, to the averaged ratios of branching fractions (see section 6.3). Typically, the largest fit systematic uncertainties arise from fixing the combinatorial slope parameter from a fit to the upper mass sideband, and from using charmed hadronic decays to model the partially reconstructed component.

The systematic uncertainty due to the fit method on the combined yield of $B^0_s \to K^0_S K^+K^-$ with the tighter selection is 12. Adding this in quadrature with the statistical uncertainty gives a yield of 207 ± 24, for which the corresponding significance, based on the ratio of the yield to the total uncertainty, is 8.6 standard deviations.

6.2 Efficiency uncertainties

Systematic uncertainties on the efficiency ratios arise from the finite size of the samples of simulated signal events, the accuracy of the corrections for data-simulation differences, and the method used to average the efficiencies.

Uncertainties on the tracking, hardware trigger, and PID corrections arise from the finite size of the data calibration samples. For the hardware-trigger correction, an additional uncertainty arises from the sample with which the average underlying energy is determined; this uncertainty is estimated by remeasuring the average underlying energy with another data calibration sample, using identified charm events instead of identified beauty events. For the PID correction, additional uncertainties arise from the finite size of the simulation sample (used to determine the signal-track kinematic distribution for the correction), and

JHEP07(2026)071

from the nonparametric kernel-density method used to describe the PID response; the latter uncertainty is estimated by varying the kernel width.

In addition, the kinematic distributions of B^0 and B_s^0 mesons may differ between simulation and data; the effect of this is tested by weighting the simulated data to match the kinematic distributions in higher-yield data samples of $B^0_{(s)} \to K^0_S h^+ h'^-$ decays and recomputing the efficiency. The change in mean efficiency after reweighting is determined for 18 separate subsamples, using combinations of three decay channels ($B^0 \to K^0_S \pi^+\pi^-$, $B^0 \to K^0_S K^+ K^-$, $B^0_s \to K^0_S K^\pm \pi^\mp$), three data-taking periods (2016, 2017, 2018), and the two K^0_S reconstruction types. The effect is found to be small, and a systematic uncertainty is assessed based on the sum in quadrature of the mean and RMS of the 18 subsamples. This uncertainty is taken to be correlated between data-taking periods.

The uncertainty on the method used to compute the weighted-average efficiency $\bar{\varepsilon}_k$ is based on the spread among the three independent estimates $\bar{\varepsilon}_{k,k'}$ (see eq. (5.2)), quantified as the RMS of $\{\bar{\varepsilon}_{k,k'} - \bar{\varepsilon}_k\}$ among all combinations k, k' for a given decay mode and K^0_S reconstruction type. (Note that there are 7×3 such combinations, for the seven data-taking periods k and the three reference periods k'.) While this does mean that some subsamples are reused in the uncertainty estimate it has the important advantage that the systematic uncertainty is stable across data-taking periods and is only mildly affected by statistical fluctuations in the smaller subsamples. This uncertainty is correlated between data-taking periods.

The average efficiency is also influenced by the choice of binning scheme for the square Dalitz plot. Instead of the baseline 10×10 binning, six other $n \times n$ grids are used (for $n = 7, 8, 9, 11, 12, 13$) and, for each grid, the average efficiency is recomputed and the difference taken with respect to that of the baseline $n = 10$ grid. This is done for each of the seven data-taking periods, for a total of 42 values, and the RMS of the distribution is taken as an estimate of the associated systematic uncertainty. This generates one uncertainty per decay mode, K^0_S reconstruction type, and selection working point (looser/tighter), and is thus correlated between data-taking periods.

6.3 Combination

For each of the five ratios of branching fractions R_i, fourteen separate measurements R_{ij} are made (from the seven data-taking periods and two K^0_S reconstruction types). In general, the agreement between all of the measurements is excellent. Only a single measurement of one branching fraction ratio shows a significant disagreement with respect to the other thirteen measurements. It is therefore assumed to be due to a fluctuation. The fourteen measurements of each branching fraction ratio are combined in a weighted average:

$$\overline{R}_i = \left[\sum_j w_{ij}\right]^{-1} \sum_j R_{ij}\, w_{ij}. \tag{6.1}$$

The weight used for each measurement is $w_{ij} = (\sigma_{ij})^{-2}$, where σ_{ij} is the sum in quadrature of the statistical and uncorrelated systematic uncertainties on the ratio R_{ij}.

The uncertainties on the individual measurements R_{ij} are propagated to the combinations $\overline{R}_i$. Other than as noted above, systematic uncertainties are assumed to be uncorrelated between subsamples and are added in quadrature. The uncertainties are summarised in

JHEP07(2026)071

Source [‰]	B^0, K^+K^-	$B^0, K^\pm\pi^\mp$	$B_s^0, \pi^+\pi^-$	B_s^0, K^+K^-	$B_s^0, K^\pm\pi^\mp$
Fit model	7.8	28.6	40.4	58.8	5.8
Tracking	0.03	0.04	< 0.01	0.07	0.03
Hardware trigger	1.3	1.0	1.0	1.4	0.7
PID	2.3	5.4	< 0.1	6.2	1.8
Kin. reweighting*	6.2	4.4	6.0	6.3	4.4
Dalitz plot*	27.3	22.6	37.3	57.2	15.3
Total systematic	29	37	55	82	17
Statistical	12	26	42	135	11
f_s/f_d*	—	—	31	31	31

Table 2. Summary of the relative systematic uncertainties on the ratios of branching fractions after taking the weighted average of the subsamples, as described in section 6.3. For each column, the decay mode in the numerator of the ratio of branching fractions is indicated by the initial b hadron and the $h^+h'^-$ combination. An asterisk indicates that the class includes uncertainties treated as correlated between different data-taking periods.

table 2. The largest sources of systematic uncertainty are the modelling of the fit components and the method to account for the efficiency variation over the Dalitz plot.

7 Results and conclusion

A dataset recorded by the LHCb detector between 2011 and 2018, corresponding to an integrated luminosity of $9\,\text{fb}^{-1}$, is used to study the $B^0_{(s)} \to K^0_S h^+ h'^-$ decay modes. The branching fraction of each decay is measured relative to that of $B^0 \to K^0_S \pi^+\pi^-$. The ratios of branching fractions are determined independently for the two K^0_S reconstruction categories and seven data-taking periods, with all such determinations being in agreement. They are then combined in a weighted average, and the results obtained are

$$\frac{\mathcal{B}(B^0 \to K^0_S K^+ K^-)}{\mathcal{B}(B^0 \to K^0_S \pi^+\pi^-)} = 0.578 \pm 0.007\,(\text{stat}) \pm 0.017\,(\text{syst})\,,$$

$$\frac{\mathcal{B}(B^0 \to K^0_S K^\pm \pi^\mp)}{\mathcal{B}(B^0 \to K^0_S \pi^+\pi^-)} = 0.1363 \pm 0.0035\,(\text{stat}) \pm 0.0051\,(\text{syst})\,,$$

$$\frac{\mathcal{B}(B^0_s \to K^0_S \pi^+\pi^-)}{\mathcal{B}(B^0 \to K^0_S \pi^+\pi^-)} = 0.269 \pm 0.011\,(\text{stat}) \pm 0.015\,(\text{syst}) \pm 0.008\,(f_s/f_d)\,,$$

$$\frac{\mathcal{B}(B^0_s \to K^0_S K^+ K^-)}{\mathcal{B}(B^0 \to K^0_S \pi^+\pi^-)} = 0.0303 \pm 0.0041\,(\text{stat}) \pm 0.0025\,(\text{syst}) \pm 0.0009\,(f_s/f_d)\,,$$

$$\frac{\mathcal{B}(B^0_s \to K^0_S K^\pm \pi^\mp)}{\mathcal{B}(B^0 \to K^0_S \pi^+\pi^-)} = 1.818 \pm 0.021\,(\text{stat}) \pm 0.031\,(\text{syst}) \pm 0.056\,(f_s/f_d)\,.$$

The decay $B^0_s \to K^0_S K^+ K^-$ is observed for the first time, with a significance exceeding six standard deviations. All measurements of branching fractions are in good agreement with the earlier LHCb determinations [68], which they supersede. The measurement of the relative

JHEP07(2026)071

branching fractions of $B^0 \to K^0_S K^\pm \pi^\mp$ and $B^0 \to K^0_S K^+ K^-$ are consistent with the world-average results [25, 26]. At present the *CP* content of the three B^0_s decays is unknown but once it is established, *e.g.* by a future amplitude analysis, the branching fraction ratios can be corrected for the modified efficiency within the estimated maximal deviation of $\pm 4\%$, corresponding to a variation of the effective B^0_s meson decay width of $\mp \Delta\Gamma_s/2$.

Using the external known value (excluding input from previous LHCb measurements that used a subset of the data considered here), $\mathcal{B}(B^0 \to K^0\pi^+\pi^-) = (4.96 \pm 0.20) \times 10^{-5}$ [26], the measured time-integrated branching fractions are

$$\begin{aligned}
\mathcal{B}(B^0 \to K^0 K^+ K^-) &= [28.6 \ \pm 0.4 \ (\text{stat}) \pm 0.8 \ (\text{syst}) \pm 1.2 \ (\text{ext})] \times 10^{-6}, \\
\mathcal{B}(B^0 \to \overline{(}\overline{K}\overline{)}^0 K^\pm \pi^\mp) &= [\ 6.76 \pm 0.17\,(\text{stat}) \pm 0.25\,(\text{syst}) \pm 0.27\,(\text{ext})] \times 10^{-6}, \\
\mathcal{B}(B^0_s \to \overline{K}^0 \pi^+ \pi^-) &= [13.3 \ \pm 0.6 \ (\text{stat}) \pm 0.7 \ (\text{syst}) \pm 0.7 \ (\text{ext})] \times 10^{-6}, \\
\mathcal{B}(B^0_s \to \overline{K}^0 K^+ K^-) &= [\ 1.50 \pm 0.20\,(\text{stat}) \pm 0.12\,(\text{syst}) \pm 0.08\,(\text{ext})] \times 10^{-6}, \\
\mathcal{B}(B^0_s \to \overline{(}\overline{K}\overline{)}^0 K^\pm \pi^\mp) &= [90.2 \ \pm 1.0 \ (\text{stat}) \pm 1.5 \ (\text{syst}) \pm 4.6 \ (\text{ext})] \times 10^{-6},
\end{aligned}$$

where 'ext' denotes the combined uncertainties on f_s/f_d and $\mathcal{B}(B^0 \to K^0\pi^+\pi^-)$. These results agree with the available predictions for these channels [4–9], and with previous experimental determinations.

Acknowledgments

We express our gratitude to our colleagues in the CERN accelerator departments for the excellent performance of the LHC. We thank the technical and administrative staff at the LHCb institutes. We acknowledge support from CERN and from the national agencies: ARC (Australia); CAPES, CNPq, FAPERJ and FINEP (Brazil); MOST and NSFC (China); CNRS/IN2P3 and CEA (France); BMFTR, DFG and MPG (Germany); INFN (Italy); NWO (Netherlands); MNiSW and NCN (Poland); MCID/IFA (Romania); MICIU and AEI (Spain); SNSF and SER (Switzerland); NASU (Ukraine); STFC (United Kingdom); DOE NP and NSF (U.S.A.). We acknowledge the computing resources that are provided by ARDC (Australia), CBPF (Brazil), CERN, IHEP and LZU (China), IN2P3 (France), KIT and DESY (Germany), INFN (Italy), SURF (Netherlands), Polish WLCG (Poland), IFIN-HH (Romania), PIC (Spain), CSCS (Switzerland), GridPP (United Kingdom), and NSF (U.S.A.). We are indebted to the communities behind the multiple open-source software packages on which we depend. Individual groups or members have received support from Key Research Program of Frontier Sciences of CAS, CAS PIFI, CAS CCEPP (China); Minciencias (Colombia); EPLANET, Marie Skłodowska-Curie Actions, ERC and NextGenerationEU (European Union); A*MIDEX, ANR, IPhU and Labex P2IO, and Région Auvergne-Rhône-Alpes (France); Alexander-von-Humboldt Foundation (Germany); ICSC (Italy); Severo Ochoa and María de Maeztu Units of Excellence, GVA, XuntaGal, GENCAT, InTalent-Inditex and Prog. Atracción Talento CM (Spain); the Leverhulme Trust, the Royal Society and UKRI (United Kingdom).

JHEP07(2026)071

Ratio	χ^2/ndf	p-value
$\mathcal{B}(B^0 \to K^0_S K^+ K^-)/\mathcal{B}(B^0 \to K^0_S \pi^+ \pi^-)$	17.9/13	16%
$\mathcal{B}(B^0 \to K^0_S K^\pm \pi^\mp)/\mathcal{B}(B^0 \to K^0_S \pi^+ \pi^-)$	6.91/13	91%
$\mathcal{B}(B^0_s \to K^0_S \pi^+ \pi^-)/\mathcal{B}(B^0 \to K^0_S \pi^+ \pi^-)$	10.5/13	65%
$\mathcal{B}(B^0_s \to K^0_S K^+ K^-)/\mathcal{B}(B^0 \to K^0_S \pi^+ \pi^-)$	33.0/13	0.17%
$\mathcal{B}(B^0_s \to K^0_S K^\pm \pi^\mp)/\mathcal{B}(B^0 \to K^0_S \pi^+ \pi^-)$	9.50/13	73%

Table 3. For each measured ratio of branching fractions, the estimated χ^2 for compatibility among subsamples, the associated number of degrees of freedom (ndf), and the corresponding p-value assuming Gaussian uncertainties.

A Fits to all subsamples

For each ratio of branching fractions, 14 separate measurements R_{ij} are made and a weighted average $\overline{R}_i$ is computed, as described in section 6.3. The same set of measurements may also be used to compute a χ^2,

$$\chi^2_i = \sum_j \left(\frac{R_{ij} - \overline{R}_i}{\sigma_{ij}} \right)^2 , \tag{A.1}$$

where σ_{ij} is the sum in quadrature of the statistical and uncorrelated systematic uncertainties on the ratio R_{ij}, implicitly assuming Gaussian uncertainties. The results are given in table 3, along with the associated p-values. All indicate good agreement, except for the ratio $\mathcal{B}(B^0_s \to K^0_S K^+ K^-)/\mathcal{B}(B^0 \to K^0_S \pi^+ \pi^-)$. For the latter, the largest contribution (9.6) comes from the 2016 data-taking period with the long K^0_S reconstruction type; all other subsamples are mutually consistent (the remaining χ^2/ndf would be 19.84/13, corresponding to a p-value of 10%). The fit to the $K^0_S K^+ K^-$ spectrum for this sample is shown in figure 4. In this instance, both the fitted yield of $B^0_s \to K^0_S K^+ K^-$ (1.5 ± 2.6 candidates) and the background in the peak region are small, with the consequence that the estimated statistical uncertainty is also low, enhancing the χ^2 contribution. This effect is reproduced in simulated pseudoexperiments emulating the 2016 LL $K^0_S K^+ K^-$ mass spectrum, in which the B^0_s signal yield is drawn from a Poisson distribution where the expected signal yield is determined from the branching ratio averaged across all subsamples, and expected yields of other components are taken from the fit to data. In fits to the pseudoexperiments, downward fluctuations in the fitted B^0_s yield are found to be correlated with lower statistical uncertainties on the yield, and hence larger normalised residuals (pulls), with the effect becoming strongly nonlinear for fitted yields in this spectrum below five units.

JHEP07(2026)071

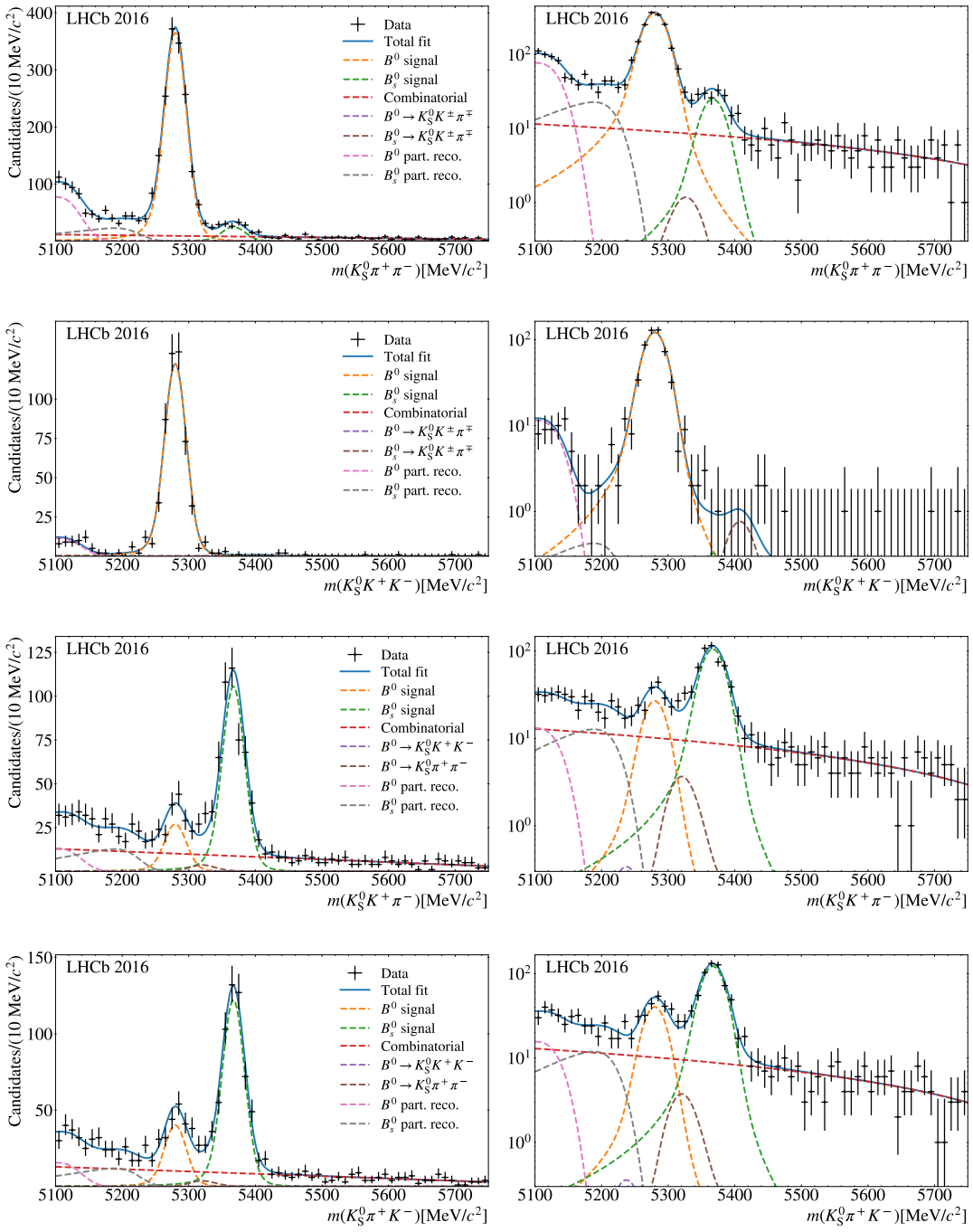

Figure 4. Mass distributions of $K^0_S h^+ h'^-$ candidates that pass the tighter selection, for the 2016 running period and the long K^0_S reconstruction type. From top to bottom, each row corresponds to a different final state: $K^0_S\pi^+\pi^-$, $K^0_S K^+ K^-$, $K^0_S K^+\pi^-$, $K^0_S\pi^+ K^-$.

JHEP07(2026)071

B Definition of the signal model

In this analysis, the probability density function (PDF) of a Crystal Ball function [58], as implemented in RooFit within Root [69], is defined as follows:

$$P_{\rm CB}(m;\mu,\sigma,n,\alpha) \equiv N \begin{cases} e^{-t^2/2} & \text{if } \ t > -|\alpha|\,, \\ \dfrac{1}{\left(\frac{n}{|\alpha|} - |\alpha| - t\right)^n} \left(\dfrac{n}{|\alpha|}\right)^n e^{-\alpha^2/2} & \text{if } \ t \leq -|\alpha|\,, \end{cases} \tag{B.1}$$

where

$$t = \begin{cases} (m-\mu)/\sigma \text{ if } \alpha > 0\,, \\ -(m-\mu)/\sigma \text{ if } \alpha < 0\,, \end{cases} \tag{B.2}$$

and where N is a normalisation factor such that the PDF has unit integral within the fit range. The signal PDF is then defined as

$$P_{\rm sig}(m;\mu,\sigma,n_L,n_R,\alpha_L,\alpha_R,f_L) \equiv f_L P_{\rm CB}(m;\mu,\sigma,n_L,\alpha_L) + (1-f_L) P_{\rm CB}(m;\mu,\sigma,n_R,-\alpha_R). \tag{B.3}$$

Fits to signal candidates in simulation are used to obtain a set of signal shape parameters, some of which are used in the fit to data as described below. Simultaneous fits are used to share parameters between different decay modes and different $K^0_{\rm S}$ reconstruction types for a given data-taking period (but not between different data-taking periods). The 22 shape parameters determined for each data-taking period are:

- Two peak position parameters $\mu(B^0)$ and $\mu(B^0_s)$;
- One width parameter $\sigma(B^0 \to K^0_{\rm S}\pi^+\pi^-, {\rm DD})$ for the decay $B^0 \to K^0_{\rm S}\pi^+\pi^-$ with the downstream $K^0_{\rm S}$ reconstruction;
- Four width ratio parameters, $\left\{r_{B^0_s},\, r_{K\pi},\, r_{KK},\, r_{\rm LL}\right\}$, which together define the width of the other signal peaks relative to $\sigma(B^0 \to K^0_{\rm S}\pi^+\pi^-, {\rm DD})$ under the assumption of factorisation:

$$\begin{aligned}
\sigma(B^0_s \to K^0_{\rm S}\pi^+\pi^-, {\rm DD}) &= \sigma(B^0 \to K^0_{\rm S}\pi^+\pi^-, {\rm DD})\, r_{B^0_s}\,, \\
\sigma(B^0 \to K^0_{\rm S}\pi^+\pi^-, {\rm LL}) &= \sigma(B^0 \to K^0_{\rm S}\pi^+\pi^-, {\rm DD})\, r_{\rm LL}\,, \\
\sigma(B^0_s \to K^0_{\rm S}\pi^+\pi^-, {\rm LL}) &= \sigma(B^0 \to K^0_{\rm S}\pi^+\pi^-, {\rm DD})\, r_{B^0_s}\, r_{\rm LL}\,, \\
\sigma(B^0 \to K^0_{\rm S}K^\pm\pi^\mp, {\rm DD}) &= \sigma(B^0 \to K^0_{\rm S}\pi^+\pi^-, {\rm DD})\, r_{K\pi}\,, \\
\sigma(B^0_s \to K^0_{\rm S}K^\pm\pi^\mp, {\rm DD}) &= \sigma(B^0 \to K^0_{\rm S}\pi^+\pi^-, {\rm DD})\, r_{B^0_s}\, r_{K\pi}\,, \\
\sigma(B^0 \to K^0_{\rm S}K^\pm\pi^\mp, {\rm LL}) &= \sigma(B^0 \to K^0_{\rm S}\pi^+\pi^-, {\rm DD})\, r_{K\pi}\, r_{\rm LL}\,, \\
\sigma(B^0_s \to K^0_{\rm S}K^\pm\pi^\mp, {\rm LL}) &= \sigma(B^0 \to K^0_{\rm S}\pi^+\pi^-, {\rm DD})\, r_{B^0_s}\, r_{K\pi}\, r_{\rm LL}\,, \\
\sigma(B^0 \to K^0_{\rm S}K^+K^-, {\rm DD}) &= \sigma(B^0 \to K^0_{\rm S}\pi^+\pi^-, {\rm DD})\, r_{KK}\,, \\
\sigma(B^0_s \to K^0_{\rm S}K^+K^-, {\rm DD}) &= \sigma(B^0 \to K^0_{\rm S}\pi^+\pi^-, {\rm DD})\, r_{B^0_s}\, r_{KK}\,, \\
\sigma(B^0 \to K^0_{\rm S}K^+K^-, {\rm LL}) &= \sigma(B^0 \to K^0_{\rm S}\pi^+\pi^-, {\rm DD})\, r_{KK}\, r_{\rm LL}\,, \\
\sigma(B^0_s \to K^0_{\rm S}K^+K^-, {\rm LL}) &= \sigma(B^0 \to K^0_{\rm S}\pi^+\pi^-, {\rm DD})\, r_{B^0_s}\, r_{KK}\, r_{\rm LL}\,;
\end{aligned}$$

JHEP07(2026)071

- Six left-hand tail parameters, which are different between final states but shared between K^0_S reconstruction types and between the B^0 and B^0_s peaks for a given final state: $\{\alpha_L(K^0_S\pi^+\pi^-), \alpha_L(K^0_S K^\pm\pi^\mp), \alpha_L(K^0_S K^+K^-)\}$ and $\{n_L(K^0_S\pi^+\pi^-), n_L(K^0_S K^\pm\pi^\mp), n_L(K^0_S K^+K^-)\}$;

- Six parameters to define the right-hand tail, each expressed as a ratio with respect to the corresponding left-hand tail parameter give above, *e.g.* $\alpha_R(K^0_S\pi^+\pi^-)/\alpha_L(K^0_S\pi^+\pi^-)$, and which are likewise different between final states but shared between K^0_S reconstruction types and between the B^0 and B^0_s peaks for a given final state;

- Three parameters describing the fraction of the signal in the component with the left-hand tail, which are different between final states but shared between K^0_S reconstruction types and between the B^0 and B^0_s peaks for a given final state: $\{f_L(K^0_S\pi^+\pi^-), f_L(K^0_S K^\pm\pi^\mp), f_L(K^0_S K^+K^-)\}$.

In the simultaneous fits to data, for each data-taking period most shape parameters are fixed according to the corresponding fits to simulation. Specifically, all of the width ratio parameters (r), all of the tail parameters ($n_L, n_R, \alpha_L, \alpha_R$), and all of the fraction parameters (f_L) are fixed. The width parameter $\sigma(B^0 \to K^0_S\pi^+\pi^-, \mathrm{DD})$ is allowed to vary, to take into account potential differences in resolution between data and simulation. Similarly, one peak position parameter $\mu(B^0)$ is allowed to vary so as to take into account potential differences in mass scale between data and simulation; the other peak position parameter is then derived as $\mu(B^0_s) = \mu(B^0) + \Delta m$, where Δm is fixed to the known difference in mass between the two states [26]. All 16 signal yields (for the four final states with $K^0_S K^+\pi^-$ and $K^0_S\pi^+K^-$ separated by charge, two K^0_S reconstruction types, and B^0 and B^0_s) for each data-taking period are free parameters.

Note that the fits described above are carried out separately at the two selection working points (loose and tight), since signal shapes and yields depend upon the selection.

C Correlation matrices

C.1 Statistical correlation matrix

The statistical correlations between the ratios of branching fractions are reported in table 4. Some branching fraction results are determined from the tight selection and others from the loose selection. The correlation matrix is computed from the tight selection, since those data are a subsample of those in the loose selection.

The correlation among yields is obtained directly from the fit and is found to be low (below 1% for most cases). Then the correlation is propagated to the ratio of yields and finally to the ratio of branching fractions. The final correlation obtained mainly results from the common denominator decay mode $B^0 \to K^0_S\pi^+\pi^-$.

The statistical covariance matrix is shown in table 5. It is obtained from table 4 using the statistical uncertainties on branching fractions reported in section 7.

JHEP07(2026)071

	$B^0 \to K^0_S K^+ K^-$	$B^0 \to K^0_S K^\pm \pi^\mp$	$B^0_s \to K^0_S \pi^+ \pi^-$	$B^0_s \to K^0_S K^+ K^-$	$B^0_s \to K^0_S K^\pm \pi^\mp$
$B^0 \to K^0_S K^+ K^-$	1.00	0.16	0.06	0.03	0.33
$B^0 \to K^0_S K^\pm \pi^\mp$	0.16	1.00	0.04	0.01	0.29
$B^0_s \to K^0_S \pi^+ \pi^-$	0.06	0.04	1.00	0.006	0.07
$B^0_s \to K^0_S K^+ K^-$	0.03	0.01	0.006	1.00	0.03
$B^0_s \to K^0_S K^\pm \pi^\mp$	0.33	0.29	0.07	0.03	1.00

Table 4. Statistical correlations, calculated as described in the text, between the ratios of branching fractions $\mathcal{B}\,(B^0_{(s)} \to K^0_S h^+ h'^-)/\mathcal{B}\,(B^0 \to K^0_S \pi^+ \pi^-)$, where the numerator decay mode is given by the row and column headings.

	$B^0 \to K^0_S K^+ K^-$	$B^0 \to K^0_S K^\pm \pi^\mp$	$B^0_s \to K^0_S \pi^+ \pi^-$	$B^0_s \to K^0_S K^+ K^-$	$B^0_s \to K^0_S K^\pm \pi^\mp$
$B^0 \to K^0_S K^+ K^-$	5.11	0.39	0.51	0.09	4.83
$B^0 \to K^0_S K^\pm \pi^\mp$	0.39	1.21	0.17	0.02	2.10
$B^0_s \to K^0_S \pi^+ \pi^-$	0.51	0.17	12.68	0.03	1.63
$B^0_s \to K^0_S K^+ K^-$	0.09	0.02	0.03	1.67	0.24
$B^0_s \to K^0_S K^\pm \pi^\mp$	4.83	2.10	1.63	0.24	42.81

$\times 10^{-5}$

Table 5. Statistical covariance matrix between the ratios of branching fractions $\mathcal{B}\,(B^0_{(s)} \to K^0_S h^+ h'^-)/\mathcal{B}\,(B^0 \to K^0_S \pi^+ \pi^-)$, where the numerator decay mode is given by the row and column headings.

C.2 Correlation matrices due to the efficiency binning scheme

Among the considered sources of systematic correlation, only the contribution associated with the efficiency-binning scheme is found to be significant. All other sources can be considered to be negligible. Since similar resonances appear in the different decays, a change in the Dalitz-plot efficiency binning might induce coherent shifts in the efficiency ratios of different signal modes, leading to correlated variations in the corresponding branching-fraction observables. In addition, the variation in the normalisation channel is common to all the ratios.

The correlations among the different signal modes due to the binning of the efficiency variation over the Dalitz plot are evaluated from the changes induced when the binning scheme is modified. For each signal mode an efficiency ratio with respect to the reference channel, $B^0 \to K^0_S \pi^+ \pi^-$, is formed in every alternative binning, data-taking period, and K^0_S reconstruction category, and the deviation of this ratio with respect to the baseline 10×10 binning is considered. For each pair of modes, all these deviations (over all binning schemes and subsamples) are treated as a sample from which the Pearson correlation coefficient is computed; these values are used as the correlation coefficients for the binning systematic and are reported in tables 6 and 7 for the tight and loose selections, respectively. The statistical uncertainties on the coefficients are obtained from the standard Fisher z-transform and quoted as $\rho_{ij} \pm \sigma_{\rho_{ij}}$. For modes that differ only by the kaon-pion charge assignment, the two-charge configurations are first averaged, so that the matrices are expressed in terms of combined $K^0_S K\pi$ observables.

Finally, to obtain the covariance matrices from the correlation matrices in tables 6 and 7, the binning-scheme systematic uncertainties propagated to the combined branching fraction ratios are used. The resulting covariance matrices for the tighter and looser optimizations are reported in tables 8 and 9, respectively.

JHEP07(2026)071

	$B^0 \to K^0_S K^+ K^-$	$B^0 \to K^0_S K^\pm \pi^\mp$	$B^0_s \to K^0_S \pi^+ \pi^-$	$B^0_s \to K^0_S K^+ K^-$	$B^0_s \to K^0_S K^\pm \pi^\mp$
$B^0 \to K^0_S K^+ K^-$	1.00	0.40 ± 0.09	0.09 ± 0.11	0.26 ± 0.10	0.33 ± 0.10
$B^0 \to K^0_S K^\pm \pi^\mp$	0.40 ± 0.09	1.00	-0.14 ± 0.11	-0.04 ± 0.11	0.53 ± 0.08
$B^0_s \to K^0_S \pi^+ \pi^-$	0.09 ± 0.11	-0.14 ± 0.11	1.00	-0.19 ± 0.11	-0.05 ± 0.11
$B^0_s \to K^0_S K^+ K^-$	0.26 ± 0.10	-0.04 ± 0.11	-0.19 ± 0.11	1.00	0.34 ± 0.10
$B^0_s \to K^0_S K^\pm \pi^\mp$	0.33 ± 0.10	0.53 ± 0.08	-0.05 ± 0.11	0.34 ± 0.10	1.00

Table 6. Correlation matrix due to the efficiency binning scheme for the tighter selection between the ratios of efficiencies $\varepsilon^{\rm sel}_{B^0_{(s)} \to K^0_S h^+ h'^-} / \varepsilon^{\rm sel}_{B^0 \to K^0_S \pi^+ \pi^-}$, where the numerator decay mode is given by the row and column headings.

	$B^0 \to K^0_S K^+ K^-$	$B^0 \to K^0_S K^\pm \pi^\mp$	$B^0_s \to K^0_S \pi^+ \pi^-$	$B^0_s \to K^0_S K^+ K^-$	$B^0_s \to K^0_S K^\pm \pi^\mp$
$B^0 \to K^0_S K^+ K^-$	1.00	0.49 ± 0.08	0.05 ± 0.11	0.22 ± 0.11	0.50 ± 0.08
$B^0 \to K^0_S K^\pm \pi^\mp$	0.49 ± 0.08	1.00	-0.16 ± 0.11	-0.06 ± 0.11	0.65 ± 0.06
$B^0_s \to K^0_S \pi^+ \pi^-$	0.05 ± 0.11	-0.16 ± 0.11	1.00	-0.17 ± 0.11	-0.09 ± 0.11
$B^0_s \to K^0_S K^+ K^-$	0.22 ± 0.11	-0.06 ± 0.11	-0.17 ± 0.11	1.00	0.37 ± 0.10
$B^0_s \to K^0_S K^\pm \pi^\mp$	0.50 ± 0.08	0.65 ± 0.06	-0.09 ± 0.11	0.37 ± 0.10	1.00

Table 7. Correlation matrix due to the efficiency binning scheme for the looser selection between the ratios of efficiencies $\varepsilon^{\rm sel}_{B^0_{(s)} \to K^0_S h^+ h'^-} / \varepsilon^{\rm sel}_{B^0 \to K^0_S \pi^+ \pi^-}$, where the numerator decay mode is given by the row and column headings.

	$B^0 \to K^0_S K^+ K^-$	$B^0 \to K^0_S K^\pm \pi^\mp$	$B^0_s \to K^0_S \pi^+ \pi^-$	$B^0_s \to K^0_S K^+ K^-$	$B^0_s \to K^0_S K^\pm \pi^\mp$
$B^0 \to K^0_S K^+ K^-$	16.83	1.16	0.50	0.35	10.35
$B^0 \to K^0_S K^\pm \pi^\mp$	1.16	0.50	−0.14	−0.01	2.88
$B^0_s \to K^0_S \pi^+ \pi^-$	0.50	−0.14	1.87	−0.09	−0.49
$B^0_s \to K^0_S K^+ K^-$	0.35	−0.01	−0.09	0.11	0.88
$B^0_s \to K^0_S K^\pm \pi^\mp$	10.35	2.88	−0.49	0.88	58.86

$\times 10^{-5}$

Table 8. Covariance matrix due to the efficiency binning scheme for the tighter selection between the ratios of efficiencies $\varepsilon^{\rm sel}_{B^0_{(s)} \to K^0_S h^+ h'^-} / \varepsilon^{\rm sel}_{B^0 \to K^0_S \pi^+ \pi^-}$, where the numerator decay mode is given by the row and column headings.

To obtain the systematic covariance between two branching fractions computed in the looser selection (e.g. $B^0 \to K^0_S K^+ K^-$ and $B^0_s \to K^0_S K^\pm \pi^\mp$), the matrix in table 9 should be used. If both branching fractions are computed in the tighter selection (e.g. $B^0 \to K^0_S K^\pm \pi^\mp$ and $B^0_s \to K^0_S K^+ K^-$), the matrix in table 8 should be used. To obtain the covariance between one branching fraction computed in the looser selection and another computed in the tighter selection (e.g. $B^0 \to K^0_S K^+ K^-$ and $B^0_s \to K^0_S K^+ K^-$), the matrix in table 8 is used as an approximation for simplicity.

JHEP07(2026)071

	$B^0 \to K^0_S K^+ K^-$	$B^0 \to K^0_S K^\pm \pi^\mp$	$B^0_s \to K^0_S \pi^+ \pi^-$	$B^0_s \to K^0_S K^+ K^-$	$B^0_s \to K^0_S K^\pm \pi^\mp$
$B^0 \to K^0_S K^+ K^-$	15.14	1.09	0.25	0.37	9.70
$B^0 \to K^0_S K^\pm \pi^\mp$	1.09	0.33	−0.11	−0.01	1.84
$B^0_s \to K^0_S \pi^+ \pi^-$	0.25	−0.11	1.57	−0.09	−0.55
$B^0_s \to K^0_S K^+ K^-$	0.37	−0.01	−0.09	0.18	0.77
$B^0_s \to K^0_S K^\pm \pi^\mp$	9.70	1.84	−0.55	0.77	24.72

$\times 10^{-5}$

Table 9. Covariance matrix due to the efficiency binning scheme for the looser selection between the ratios of efficiencies $\varepsilon^{\rm sel}_{B^0_{(s)} \to K^0_S h^+ h'^-} / \varepsilon^{\rm sel}_{B^0 \to K^0_S \pi^+ \pi^-}$, where the numerator decay mode is given by the row and column headings.

Data Availability Statement. Data associated with the plots in this publication are made available on the CERN Document Server at https://cds.cern.ch/record/2956321.

Code Availability Statement. This article has no associated code or the code will not be deposited.

Open Access. This article is distributed under the terms of the Creative Commons Attribution License (CC-BY4.0), which permits any use, distribution and reproduction in any medium, provided the original author(s) and source are credited.

References

[1] Y. Grossman and M.P. Worah, *CP asymmetries in B decays with new physics in decay amplitudes*, *Phys. Lett. B* **395** (1997) 241 [hep-ph/9612269] [INSPIRE].

[2] D. London and A. Soni, *Measuring the CP angle Beta in hadronic $b \to s$ penguin decays*, *Phys. Lett. B* **407** (1997) 61 [hep-ph/9704277] [INSPIRE].

[3] M. Ciuchini et al., *CP violating B decays in the standard model and supersymmetry*, *Phys. Rev. Lett.* **79** (1997) 978 [hep-ph/9704274] [INSPIRE].

[4] H.-Y. Cheng and C.-K. Chua, *Branching fractions and direct CP violation in charmless three-body decays of B mesons*, *Phys. Rev. D* **88** (2013) 114014 [arXiv:1308.5139] [INSPIRE].

[5] H.-Y. Cheng and C.-K. Chua, *Charmless three-body decays of B_s mesons*, *Phys. Rev. D* **89** (2014) 074025 [arXiv:1401.5514] [INSPIRE].

[6] Y. Li, *Branching fractions and direct CP asymmetries of $\bar{B}^0_s \to K^0 h^+ h'^- (h^{(\prime)} = K, \pi)$ decays*, *Sci. China Phys. Mech. Astron.* **58** (2015) 031001 [arXiv:1401.5948] [INSPIRE].

[7] Y. Li, *Comprehensive study of $\overline{B}^0 \to K^0(\overline{K}^0) K^\mp \pi^\pm$ decays in the factorization approach*, *Phys. Rev. D* **89** (2014) 094007 [arXiv:1402.6052] [INSPIRE].

[8] W.-F. Wang and H.-N. Li, *Quasi-two-body decays $B \to K\rho \to K\pi\pi$ in perturbative QCD approach*, *Phys. Lett. B* **763** (2016) 29 [arXiv:1609.04614] [INSPIRE].

[9] Y. Li, A.-J. Ma, W.-F. Wang and Z.-J. Xiao, *Quasi-two-body decays $B_{(s)} \to P\rho'(1450), P\rho''(1700) \to P\pi\pi$ in the perturbative QCD approach*, *Phys. Rev. D* **96** (2017) 036014 [arXiv:1704.07566] [INSPIRE].

[10] X.-G. He, G.-N. Li and D. Xu, *SU(3) and isospin breaking effects on $B \to PPP$ amplitudes*, *Phys. Rev. D* **91** (2015) 014029 [arXiv:1410.0476] [INSPIRE].

JHEP07(2026)071

[11] Belle collaboration, *Study of B meson decays to three body charmless hadronic final states*, *Phys. Rev. D* **69** (2004) 012001 [hep-ex/0307082] [INSPIRE].

[12] Belle collaboration, *Dalitz analysis of three-body charmless $B^0 \to K^0\pi^+\pi^-$ decay*, *Phys. Rev. D* **75** (2007) 012006 [hep-ex/0610081] [INSPIRE].

[13] BaBar collaboration, *Time-dependent amplitude analysis of $B^0 \to K^0_S\pi^+\pi^-$*, *Phys. Rev. D* **80** (2009) 112001 [arXiv:0905.3615] [INSPIRE].

[14] BaBar collaboration, *Observation of the rare decay $B^0 \to K^0_s K^\pm\pi^\mp$*, *Phys. Rev. D* **82** (2010) 031101 [arXiv:1003.0640] [INSPIRE].

[15] BaBar collaboration, *Study of CP violation in Dalitz-plot analyses of $B^0 \to K^+K^-K^0_S$, $B^+ \to K^+K^-K^+$, and $B^+ \to K^0_S K^0_S K^+$*, *Phys. Rev. D* **85** (2012) 112010 [arXiv:1201.5897] [INSPIRE].

[16] LHCb collaboration, *Study of $B^0_{(s)} \to K^0_S h^+ h'^-$ decays with first observation of $B^0_s \to K^0_S K^\pm\pi^\mp$ and $B^0_s \to K^0_S\pi^+\pi^-$*, *JHEP* **10** (2013) 143 [arXiv:1307.7648] [INSPIRE].

[17] LHCb collaboration, *Updated branching fraction measurements of $B^0_{(s)} \to K^0_S h^+ h'^-$ decays*, *JHEP* **11** (2017) 027 [arXiv:1707.01665] [INSPIRE].

[18] N. Cabibbo, *Unitary symmetry and leptonic decays*, *Phys. Rev. Lett.* **10** (1963) 531 [INSPIRE].

[19] M. Kobayashi and T. Maskawa, *CP violation in the renormalizable theory of weak interaction*, *Prog. Theor. Phys.* **49** (1973) 652 [INSPIRE].

[20] M. Beneke, *Corrections to $\sin(2\beta)$ from CP asymmetries in $B^0 \to (\pi^0, \rho^0, \eta, \eta', \omega, \phi)\, K_S$ decays*, *Phys. Lett. B* **620** (2005) 143 [hep-ph/0505075] [INSPIRE].

[21] G. Buchalla, G. Hiller, Y. Nir and G. Raz, *The pattern of CP asymmetries in $B \to s$ transitions*, *JHEP* **09** (2005) 074 [hep-ph/0503151] [INSPIRE].

[22] R. Dutta and S. Gardner, *CP asymmetries in $B \to f_0 K_S$ decays*, *Phys. Rev. D* **78** (2008) 034021 [arXiv:0805.1963] [INSPIRE].

[23] Belle collaboration, *Time-dependent Dalitz plot measurement of CP parameters in $B^0 \to K^0_s\pi^+\pi^-$ decays*, *Phys. Rev. D* **79** (2009) 072004 [arXiv:0811.3665] [INSPIRE].

[24] Belle collaboration, *Measurement of CP violating asymmetries in $B^0 \to K^+K^-K^0_S$ decays with a time-dependent Dalitz approach*, *Phys. Rev. D* **82** (2010) 073011 [arXiv:1007.3848] [INSPIRE].

[25] Heavy Flavor Averaging Group (HFLAV) collaboration, *Averages of b-hadron, c-hadron, and τ-lepton properties as of 2023*, *Phys. Rev. D* **113** (2026) 012008 [arXiv:2411.18639] [INSPIRE].

[26] Particle Data Group collaboration, *Review of particle physics*, *Phys. Rev. D* **110** (2024) 030001 [INSPIRE].

[27] M. Ciuchini, M. Pierini and L. Silvestrini, *$B_s \to K^{(*)0}\bar{K}^{(*)0}$ decays: the golden channels for new physics searches*, *Phys. Rev. Lett.* **100** (2008) 031802 [hep-ph/0703137] [INSPIRE].

[28] M. Ciuchini, M. Pierini and L. Silvestrini, *New bounds on the CKM matrix from $B \to K\pi\pi$ Dalitz plot analyses*, *Phys. Rev. D* **74** (2006) 051301 [hep-ph/0601233] [INSPIRE].

[29] M. Gronau, D. Pirjol, A. Soni and J. Zupan, *Improved method for CKM constraints in charmless three-body B and B_s decays*, *Phys. Rev. D* **75** (2007) 014002 [hep-ph/0608243] [INSPIRE].

[30] J. Charles, S. Descotes-Genon, J. Ocariz and A. Pérez Pérez, *Disentangling weak and strong interactions in $B \to K^*(\to K\pi)\pi$ Dalitz-plot analyses*, *Eur. Phys. J. C* **77** (2017) 561 [arXiv:1704.01596] [INSPIRE].

JHEP07(2026)071

[31] BaBar collaboration, *Amplitude analysis of $B^0 \to K^+\pi^-\pi^0$ and evidence of direct CP violation in $B \to K^*\pi$ decays*, *Phys. Rev. D* **83** (2011) 112010 [arXiv:1105.0125] [INSPIRE].

[32] BaBar collaboration, *Evidence for CP violation in $B^+ \to K^*(892)^+\pi^0$ from a Dalitz plot analysis of $B^+ \to K^0_S\pi^+\pi^0$ decays*, *Phys. Rev. D* **96** (2017) 072001 [arXiv:1501.00705] [INSPIRE].

[33] N. Rey-Le Lorier and D. London, *Measuring gamma with $B \to K\pi\pi$ and $B \to KK\bar{k}$ decays*, *Phys. Rev. D* **85** (2012) 016010 [arXiv:1109.0881] [INSPIRE].

[34] B. Bhattacharya, M. Imbeault and D. London, *Extraction of the CP-violating phase γ using $B \to K\pi\pi$ and $B \to KK\bar{K}$ decays*, *Phys. Lett. B* **728** (2014) 206 [arXiv:1303.0846] [INSPIRE].

[35] B. Bhattacharya and D. London, *Using U spin to extract γ from charmless $B \to PPP$ decays*, *JHEP* **04** (2015) 154 [arXiv:1503.00737] [INSPIRE].

[36] E. Bertholet et al., *Extraction of the CKM phase γ using charmless 3-body decays of B mesons*, *Phys. Rev. D* **99** (2019) 114011 [arXiv:1812.06194] [INSPIRE].

[37] M. Ciuchini, M. Pierini and L. Silvestrini, *Hunting the CKM weak phase with time-integrated Dalitz analyses of $B_s \to KK\pi$ and $B_s \to K\pi\pi$ decays*, *Phys. Lett. B* **645** (2007) 201 [hep-ph/0602207] [INSPIRE].

[38] LHCb collaboration, *Measurement of the b-quark production cross-section in 7 and 13 TeV pp collisions*, *Phys. Rev. Lett.* **118** (2017) 052002 [*Erratum ibid.* **119** (2017) 169901] [arXiv:1612.05140] [INSPIRE].

[39] K. De Bruyn et al., *Branching ratio measurements of B_s decays*, *Phys. Rev. D* **86** (2012) 014027 [arXiv:1204.1735] [INSPIRE].

[40] LHCb collaboration, *The LHCb detector at the LHC*, 2008 *JINST* **3** S08005 [INSPIRE].

[41] LHCb collaboration, *LHCb detector performance*, *Int. J. Mod. Phys. A* **30** (2015) 1530022 [arXiv:1412.6352] [INSPIRE].

[42] T. Sjostrand, S. Mrenna and P.Z. Skands, *A brief introduction to PYTHIA 8.1*, *Comput. Phys. Commun.* **178** (2008) 852 [arXiv:0710.3820] [INSPIRE].

[43] T. Sjostrand, S. Mrenna and P.Z. Skands, *PYTHIA 6.4 physics and manual*, *JHEP* **05** (2006) 026 [hep-ph/0603175] [INSPIRE].

[44] LHCb collaboration, *Handling of the generation of primary events in Gauss, the LHCb simulation framework*, *J. Phys. Conf. Ser.* **331** (2011) 032047 [INSPIRE].

[45] D.J. Lange, *The EvtGen particle decay simulation package*, *Nucl. Instrum. Meth. A* **462** (2001) 152 [INSPIRE].

[46] N. Davidson, T. Przedzinski and Z. Was, *PHOTOS interface in C++: technical and physics documentation*, *Comput. Phys. Commun.* **199** (2016) 86 [arXiv:1011.0937] [INSPIRE].

[47] J. Allison et al., *GEANT4 developments and applications*, *IEEE Trans. Nucl. Sci.* **53** (2006) 270 [INSPIRE].

[48] GEANT4 collaboration, *GEANT4 — a simulation toolkit*, *Nucl. Instrum. Meth. A* **506** (2003) 250 [INSPIRE].

[49] LHCb collaboration, *The LHCb simulation application, Gauss: design, evolution and experience*, *J. Phys. Conf. Ser.* **331** (2011) 032023 [INSPIRE].

[50] L. Anderlini et al., *The PIDCalib package*, LHCb-PUB-2016-021 (2016) [INSPIRE].

JHEP07(2026)071

[51] A. Poluektov, *Kernel density estimation of a multidimensional efficiency profile*, 2015 *JINST* **10** P02011 [arXiv:1411.5528] [INSPIRE].

[52] R. Aaij et al., *The LHCb trigger and its performance in 2011*, 2013 *JINST* **8** P04022 [arXiv:1211.3055] [INSPIRE].

[53] V.V. Gligorov and M. Williams, *Efficient, reliable and fast high-level triggering using a bonsai boosted decision tree*, 2013 *JINST* **8** P02013 [arXiv:1210.6861] [INSPIRE].

[54] T. Likhomanenko et al., *LHCb topological trigger reoptimization*, *J. Phys. Conf. Ser.* **664** (2015) 082025 [arXiv:1510.00572] [INSPIRE].

[55] T. Chen and C. Guestrin, *XGBoost: a scalable tree boosting system*, arXiv:1603.02754 [DOI:10.1145/2939672.2939785] [INSPIRE].

[56] L. Breiman, J. Friedman, R.A. Olshen and C.J. Stone, *Classification and regression trees*, Chapman and Hall/CRC (2017) [DOI:10.1201/9781315139470] [INSPIRE].

[57] G. Punzi, *Sensitivity of searches for new signals and its optimization*, *eConf C* **030908** (2003) MODT002 [physics/0308063] [INSPIRE].

[58] T. Skwarnicki, *A study of the radiative CASCADE transitions between the Upsilon-Prime and Upsilon resonances*, Ph.D. thesis, INP, Cracow, Poland (1986) [INSPIRE].

[59] ARGUS collaboration, *Exclusive hadronic decays of B mesons*, *Z. Phys. C* **48** (1990) 543 [INSPIRE].

[60] R.J. Barlow, *Event classification using weighting methods*, *J. Comput. Phys.* **72** (1987) 202 [INSPIRE].

[61] M. Pivk and F.R. Le Diberder, *SPlot: a statistical tool to unfold data distributions*, *Nucl. Instrum. Meth. A* **555** (2005) 356 [physics/0402083] [INSPIRE].

[62] LHCb collaboration, *Precise measurement of the f_s/f_d ratio of fragmentation fractions and of B^0_s decay branching fractions*, *Phys. Rev. D* **104** (2021) 032005 [arXiv:2103.06810] [INSPIRE].

[63] R.H. Dalitz, *On the analysis of tau-meson data and the nature of the tau-meson*, *Phil. Mag. Ser. 7* **44** (1953) 1068 [INSPIRE].

[64] LHCb collaboration, *Amplitude analysis of $B^0_s \to K^0_S K^\pm \pi^\mp$ decays*, *JHEP* **06** (2019) 114 [arXiv:1902.07955] [INSPIRE].

[65] BABAR collaboration, *An amplitude analysis of the decay $B^\pm \to \pi^\pm\pi^\pm\pi^\mp$*, *Phys. Rev. D* **72** (2005) 052002 [hep-ex/0507025] [INSPIRE].

[66] LHCb collaboration, *Measurement of the track reconstruction efficiency at LHCb*, 2015 *JINST* **10** P02007 [arXiv:1408.1251] [INSPIRE].

[67] D. Martínez Santos and F. Dupertuis, *Mass distributions marginalized over per-event errors*, *Nucl. Instrum. Meth. A* **764** (2014) 150 [arXiv:1312.5000] [INSPIRE].

[68] LHCb collaboration, *Observation of $B^+_c \to J/\psi D^+_s$ and $B^+_c \to J/\psi D^{*+}_s$ decays*, *Phys. Rev. D* **87** (2013) 112012 [*Addendum ibid.* **89** (2014) 019901] [arXiv:1304.4530] [INSPIRE].

[69] R. Brun and F. Rademakers, *ROOT — an object oriented data analysis framework*, *Nucl. Instrum. Meth. A* **389** (1997) 81 [INSPIRE].

[70] LHCb collaboration, *Data associated with the plots in this publication*, https://cds.cern.ch/record/2956321.

JHEP07(2026)071

The LHCb collaboration

R. Aaij[38], A.S.W. Abdelmotteleb[57], C. Abellan Beteta[51], F. Abudinén[57], T. Ackernley[61], A.A. Adefisoye[69], B. Adeva[47], M. Adinolfi[55], P. Adlarson[82], H. Afsharnia[11], C. Agapopoulou[14], C.A. Aidala[83], Z. Ajaltouni[11], S. Akar[66], K. Akiba[38], P. Albicocco[28], J. Albrecht[19,g], F. Alessio[49], Z. Aliouche[63], P. Alvarez Cartelle[56], R. Amalric[16], S. Amato[3], J.L. Amey[55], Y. Amhis[14,49], L. An[6], L. Anderlini[27], M. Andersson[51], A. Andreianov[44], P. Andreola[51], M. Andreotti[26], D. Andreou[69], A. Anelli[31,p], D. Ao[7], F. Archilli[37,w], M. Argenton[26], S. Arguedas Cuendis[9,49], A. Artamonov[44], M. Artuso[69], E. Aslanides[13], R. Ataíde Da Silva[50], M. Atzeni[65], B. Audurier[12], D. Bacher[64], I. Bachiller Perea[10], S. Bachmann[22], M. Bachmayer[50], J.J. Back[57], P. Baladron Rodriguez[47], V. Balagura[15], W. Baldini[26], L. Balzani[19], H. Bao[7], J. Baptista de Souza Leite[61], C. Barbero Pretel[47,12], M. Barbetti[27], I.R. Barbosa[70], R.J. Barlow[63,63,†], M. Barnyakov[25], S. Barsuk[14], W. Barter[59], M. Bartolini[56], J. Bartz[69], J.M. Basels[17], S. Bashir[40], G. Bassi[35,t], B. Batsukh[5], P.B. Battista[14], A. Bay[50], A. Beck[57], M. Becker[19], F. Bedeschi[35], I.B. Bediaga[2], N.A. Behling[19], S. Belin[47], V. Bellee[51], K. Belous[44], I. Belov[29], I. Belyaev[36], E. Ben-Haim[16], G. Benane[13], G. Bencivenni[28], A. Berezhnoy[44], R. Bernet[51], S. Bernet Andres[46], E. Bertholet[16], A. Bertolin[33], C. Betancourt[51], F. Betti[59], J. Bex[56], Ia. Bezshyiko[51], J. Bhom[41], M.S. Bieker[19], N.V. Biesuz[26], P. Billoir[16], A. Biolchini[38], M. Birch[62], F.C.R. Bishop[10], A. Bitadze[63], A. Bizzeti[27,q], T. Blake[57], F. Blanc[50], J.E. Blank[19], S. Blusk[69], V. Bocharnikov[44], J.A. Boelhauve[19], O. Boente Garcia[15], T. Boettcher[66], A. Bohare[59], A. Boldyrev[44], C. Bolognani[79], R. Bolzonella[26,m], N. Bondar[44], A. Bordelius[49], F. Borgato[33,r], S. Borghi[63], M. Borsato[31,p], J.T. Borsuk[41], S.A. Bouchiba[50], M. Bovill[64], T.J.V. Bowcock[61], A. Boyer[49], C. Bozzi[26], A. Brea Rodriguez[50], N. Breer[19], J. Brodzicka[41], A. Brossa Gonzalo[57,47,45,†], J. Brown[61], D. Brundu[32], E. Buchanan[59], A. Buonaura[51], L. Buonincontri[33,r], A.T. Burke[63], C. Burr[49], J.S. Butter[56], J. Buytaert[49], W. Byczynski[49], S. Cadeddu[32], H. Cai[74], A. Caillet[16], R. Calabrese[26,m], S. Calderon Ramirez[9], L. Calefice[45], S. Cali[28], M. Calvi[31,p], M. Calvo Gomez[46], P. Camargo Magalhaes[2,a], J.I. Cambon Bouzas[47], P. Campana[28], D.H. Campora Perez[79], A.F. Campoverde Quezada[7], S. Capelli[31], L. Capriotti[26], R. Caravaca-Mora[9], A. Carbone[25,k], L. Carcedo Salgado[47], R. Cardinale[29,n], A. Cardini[32], P. Carniti[31,p], L. Carus[22], A. Casais Vidal[65], R. Caspary[22], G. Casse[61], M. Cattaneo[49], G. Cavallero[26,49], V. Cavallini[26,m], S. Celani[22], D. Cervenkov[64], S. Cesare[30,o], A.J. Chadwick[61], I. Chahrour[83], M. Charles[16], Ph. Charpentier[49], E. Chatzianagnostou[38], M. Chefdeville[10], C. Chen[13], S. Chen[5], Z. Chen[7], A. Chernov[41], S. Chernyshenko[53], X. Chiotopoulos[79], V. Chobanova[81], S. Cholak[50], M. Chrzaszcz[41], A. Chubykin[44], V. Chulikov[44], P. Ciambrone[28], X. Cid Vidal[47], G. Ciezarek[49], P. Cifra[49], P.E.L. Clarke[59], M. Clemencic[49], H.V. Cliff[56], J. Closier[49], C. Cocha Toapaxi[22], V. Coco[49], J. Cogan[13], E. Cogneras[11], L. Cojocariu[43], P. Collins[49], T. Colombo[49], M. Colonna[19], A. Comerma-Montells[45], L. Congedo[24], A. Contu[32], N. Cooke[60], I. Corredoira[47], A. Correia[16], G. Corti[49], J. Cottee Meldrum[55], B. Couturier[49], D.C. Craik[51], M. Cruz Torres[2,h], E. Curras Rivera[50], R. Currie[59], C. D'Ambrosio[49], P. d'Argent[24], C.L. Da Silva[68], S. Dadabaev[44], L. Dai[71], X. Dai[6], E. Dall'Occo[49],

JHEP07(2026)071

J. Dalseno[47], J. Daniel[11], A. Danilina[44], A. Davidson[57], J.E. Davies[63], A. Davis[63], O. De Aguiar Francisco[63], C. De Angelis[32,l], F. De Benedetti[49], J. de Boer[38], K. De Bruyn[78], S. De Capua[63], M. De Cian[22,49], U. De Freitas Carneiro Da Graca[2,b], E. De Lucia[28], J.M. De Miranda[2], L. De Paula[3], M. De Serio[24,i], P. De Simone[28], F. De Vellis[19], J.A. de Vries[79], F. Debernardis[24], D. Decamp[10], V. Dedu[13], S. Dekkers[1], L. Del Buono[16], B. Delaney[65], H.-P. Dembinski[19], J. Deng[8], V. Denysenko[51], O. Deschamps[11], F. Dettori[32,l], B. Dey[77], P. Di Nezza[28], I. Diachkov[44], S. Didenko[44], S. Ding[69], L. Dittmann[22], V. Dobishuk[53], A.D. Docheva[60], C. Dong[4,c], A.M. Donohoe[23], F. Dordei[32], A.C. dos Reis[2], A.D. Dowling[69], W. Duan[72], P. Duda[80], M.W. Dudek[41], L. Dufour[49], V. Duk[34], P. Durante[49], M.M. Duras[80], J.M. Durham[68], O.D. Durmus[77], A. Dziurda[41], A. Dzyuba[44], S. Easo[58], E. Eckstein[18], U. Egede[1], A. Egorychev[44], V. Egorychev[44], S. Eisenhardt[59], E. Ejopu[63], L. Eklund[82], M. Elashri[66], J. Ellbracht[19], S. Ely[62], A. Ene[43], E. Epple[66], J. Eschle[69], S. Esen[22], T. Evans[63], Q. Führing[19,56,g], F. Fabiano[32,l], L.N. Falcao[2], Y. Fan[7], B. Fang[7], L. Fantini[34,49,s], M. Faria[50], K. Farmer[59], D. Fazzini[31,p], L. Felkowski[80], M. Feng[5,7], M. Feo[19,49], A. Fernandez Casani[48], M. Fernandez Gomez[47], A.D. Fernez[67], F. Ferrari[25,k], F. Ferreira Rodrigues[3], M. Ferrillo[51], M. Ferro-Luzzi[49], S. Filippov[44], R.A. Fini[24], M. Fiorini[26,m], M. Firlej[40], K.L. Fischer[64], D.S. Fitzgerald[83], C. Fitzpatrick[63], T. Fiutowski[40], F. Fleuret[15], M. Fontana[25], L.A. Foreman[63], R. Forty[49], D. Foulds-Holt[56], V. Franco Lima[3], M. Franco Sevilla[67], M. Frank[49], E. Franzoso[26,m], G. Frau[63], C. Frei[49], D.A. Friday[63], J. Fu[7], Y. Fujii[1], T. Fulghesu[16], C. Göbel[70], P.A. Günther[22], E. Gabriel[38], G. Galati[24], M.D. Galati[38], A. Gallas Torreira[47], D. Galli[25,k], S. Gambetta[59], M. Gandelman[3], P. Gandini[30], B. Ganie[63], H. Gao[7], R. Gao[64], T.Q. Gao[56], Y. Gao[8], Y. Gao[6], Y. Gao[8], J. García Pardiñas[49], L.M. Garcia Martin[50], P. Garcia Moreno[45], K.G. Garg[8], L. Garrido[45], C. Gaspar[49], R.E. Geertsema[38], L.L. Gerken[19], E. Gersabeck[63], M. Gersabeck[20], T. Gershon[57], S. Ghizzo[29,n], Z. Ghorbanimoghaddam[55], L. Giambastiani[33,r], F.I. Giasemis[16,f], V. Gibson[56], H.K. Giemza[42], A.L. Gilman[64], M. Giovannetti[28], A. Gioventù[45], L. Girardey[63,58], P. Gironella Gironell[45], C. Giugliano[26,m], M.A. Giza[41], E.L. Gkougkousis[62], F.C. Glaser[14,22], V.V. Gligorov[16,49], E. Golobardes[46], D. Golubkov[44], A. Golutvin[62,49,44], S. Gomez Fernandez[45], F. Goncalves Abrantes[64], M. Goncerz[41], G. Gong[4,c], J.A. Gooding[19], I.V. Gorelov[44], C. Gotti[31], J.P. Grabowski[18], T. Grammatico[16], L.A. Granado Cardoso[49], E. Graugés[45], E. Graverini[50,u], L. Grazette[57], G. Graziani[27], A.T. Grecu[43], L.M. Greeven[38], N.A. Grieser[66], L. Grillo[60], S. Gromov[44], C. Gu[15], M. Guarise[26], L. Guerry[11], M. Guittiere[14], V. Guliaeva[44], A.-K. Guseinov[50], E. Gushchin[44], Y. Guz[6,49,44], T. Gys[49], K. Habermann[18], T. Hadavizadeh[1], C. Hadjivasiliou[67], G. Haefeli[50], C. Haen[49], J. Haimberger[49], M. Hajheidari[49], G. Hallett[57], M.M. Halvorsen[49], P.M. Hamilton[67], J. Hammerich[61], Q. Han[8], X. Han[22,49], S. Hansmann-Menzemer[22], L. Hao[7], N. Harnew[64], M. Hartmann[14], S. Hashmi[40], J. He[7,d], F. Hemmer[49], C. Henderson[66], R.D.L. Henderson[1,57], A.M. Hennequin[49], K. Hennessy[61], L. Henry[50], J. Herd[62], P. Herrero Gascon[22], J. Heuel[17], A. Hicheur[3], G. Hijano Mendizabal[51], D. Hill[50], J. Horswill[63], R. Hou[8], Y. Hou[11], N. Howarth[61], J. Hu[72], W. Hu[6], X. Hu[4,c], W. Huang[7], W. Hulsbergen[38],

JHEP07(2026)071

R.J. Hunter[57], M. Hushchyn[44], D. Hutchcroft[61], M. Idzik[40], D. Ilin[44], P. Ilten[66], A. Inglessi[44], A. Iniukhin[44], A. Ishteev[44], K. Ivshin[44], R. Jacobsson[49], H. Jage[17], S.J. Jaimes Elles[48,75], S. Jakobsen[49], E. Jans[38], B.K. Jashal[48], A. Jawahery[67,49], V. Jevtic[19], E. Jiang[67], X. Jiang[5,7], Y. Jiang[7], Y.J. Jiang[6], M. John[64], A. John Rubesh Rajan[23], D. Johnson[54], C.R. Jones[56], T.P. Jones[57], S. Joshi[42], B. Jost[49], J. Juan Castella[56], N. Jurik[49], I. Juszczak[41], D. Kaminaris[50], S. Kandybei[52], M. Kane[59], Y. Kang[4,c], C. Kar[11], M. Karacson[49], D. Karpenkov[44], A. Kauniskangas[50], J.W. Kautz[66], M.K. Kazanecki[41], F. Keizer[49], M. Kenzie[56], T. Ketel[38], B. Khanji[69], A. Kharisova[44], S. Kholodenko[35,49], G. Khreich[14], T. Kirn[17], V.S. Kirsebom[31,p], O. Kitouni[65], S. Klaver[39], N. Kleijne[35,t], K. Klimaszewski[42], M.R. Kmiec[42], S. Koliiev[53], L. Kolk[19], A. Konoplyannikov[44], P. Kopciewicz[40,49], P. Koppenburg[38], M. Korolev[44], I. Kostiuk[38], O. Kot[53], S. Kotriakhova[32], A. Kozachuk[44], P. Kravchenko[44], L. Kravchuk[44], M. Kreps[57], P. Krokovny[44], W. Krupa[69], W. Krzemien[42], O. Kshyvanskyi[53], S. Kubis[80], M. Kucharczyk[41], V. Kudryavtsev[44], E. Kulikova[44], A. Kupsc[82], B. Kutsenko[13], S. López Soliño[47], D. Lacarrere[49], P. Laguarta Gonzalez[45], A. Lai[32], A. Lampis[32], D. Lancierini[56], C. Landesa Gomez[47], J.J. Lane[1], R. Lane[55], G. Lanfranchi[28], C. Langenbruch[22], J. Langer[19], O. Lantwin[44], T. Latham[57], F. Lazzari[35,u], C. Lazzeroni[54], R. Le Gac[13], H. Lee[61], R. Lefèvre[11], A. Leflat[44], S. Legotin[44], M. Lehuraux[57], E. Lemos Cid[49], O. Leroy[13], T. Lesiak[41], E.D. Lesser[49], B. Leverington[22], A. Li[4,c], C. Li[13], H. Li[72], K. Li[8], L. Li[63], M. Li[8], P. Li[7], P.-R. Li[73], Q. Li[5,7], S. Li[8], T. Li[5,e], T. Li[72], Y. Li[8], Y. Li[5], Z. Lian[4,c], X. Liang[69], S. Libralon[48], C. Lin[7], T. Lin[58], R. Lindner[49], V. Lisovskyi[50], R. Litvinov[32,49], F.L. Liu[1], G. Liu[72], K. Liu[73], S. Liu[5,7], W. Liu[8], Y. Liu[59], Y. Liu[73], Y.L. Liu[62], A. Lobo Salvia[45], A. Loi[32], J. Lomba Castro[47], T. Long[56], J.H. Lopes[3], A. Lopez Huertas[45], Q. Lu[15], C. Lucarelli[27], D. Lucchesi[33,r], M. Lucio Martinez[79], V. Lukashenko[38,53], Y. Luo[6], A. Lupato[33,j], E. Luppi[26,m], K. Lynch[23], X.-R. Lyu[7], K. Müller[51], G.M. Ma[4,c], S. Maccolini[19], F. Machefert[14], F. Maciuc[43], B. Mack[69], I. Mackay[64], L.M. Mackey[69], L.R. Madhan Mohan[56], M.J. Madurai[54], A. Maevskiy[44], D. Magdalinski[38], D. Maisuzenko[44], M.W. Majewski[40], J.J. Malczewski[41], S. Malde[64], L. Malentacca[49], A. Malinin[44], T. Maltsev[44,44], G. Manca[32,l], G. Mancinelli[13], C. Mancuso[30,14,o], R. Manera Escalero[45], F.M. Manganella[37], D. Manuzzi[25], D. Marangotto[30,o], J.F. Marchand[10], R. Marchevski[50], U. Marconi[25], E. Mariani[16], S. Mariani[49], C. Marin Benito[45,49], J. Marks[22], A.M. Marshall[55], L. Martel[64], G. Martelli[34,s], G. Martellotti[36], L. Martinazzoli[49], M. Martinelli[31,p], D. Martinez Santos[47], F. Martinez Vidal[48], A. Massafferri[2], R. Matev[49], A. Mathad[49], V. Matiunin[44], C. Matteuzzi[69], K.R. Mattioli[15], A. Mauri[62], E. Maurice[15], J. Mauricio[45], P. Mayencourt[50], J. Mazorra de Cos[48], M. Mazurek[42], M. McCann[62], L. Mcconnell[23], T.H. McGrath[63], N.T. McHugh[60], A. McNab[63], R. McNulty[23], B. Meadows[66], G. Meier[19], D. Melnychuk[42], F.M. Meng[4,c], M. Merk[38,79], A. Merli[50], L. Meyer Garcia[67], D. Miao[5,7], H. Miao[7], M. Mikhasenko[76], D.A. Milanes[75], A. Minotti[31,p], E. Minucci[69], T. Miralles[11], B. Mitreska[19], D.S. Mitzel[19], A. Modak[58], R.A. Mohammed[64], R.D. Moise[17], S. Mokhnenko[44], E.F. Molina Cardenas[83], T. Mombächer[49], M. Monk[57,1], S. Monteil[11], A. Morcillo Gomez[47], G. Morello[28],

JHEP07(2026)071

M.J. Morello[35,t], M.P. Morgenthaler[22], J. Moron[40], A.B. Morris[49], A.G. Morris[13], R. Mountain[69], H. Mu[4,c], Z. Mu[6], F. Muñoz-Rojas[9], E. Muhammad[57], F. Muheim[59], M. Mulder[78], R. Murta[62], P. Naik[61], T. Nakada[50], R. Nandakumar[58], T. Nanut[49], I. Nasteva[3], M. Needham[59], N. Neri[30,o], S. Neubert[18], N. Neufeld[49], P. Neustroev[44], J. Nicolini[19,14], D. Nicotra[79], E.M. Niel[50], N. Nikitin[44], Q. Niu[73], P. Nogarolli[3], P. Nogga[18], C. Normand[55], J. Novoa Fernandez[47], G. Nowak[66], C. Nunez[83], H.N. Nur[60], R.H. O'Neil[59], A. Oblakowska-Mucha[40], V. Obraztsov[44], T. Oeser[17], S. Okamura[26,m], A. Okhotnikov[44], O. Okhrimenko[53], R. Oldeman[32,l], F. Oliva[59], M. Olocco[19], C.J.G. Onderwater[79], J.S. Ordonez Soto[75], D. Osthues[19], J.M. Otalora Goicochea[3], P. Owen[51], A. Oyanguren[48], O. Ozcelik[59], F. Paciolla[35,x], A. Padee[42], K.O. Padeken[18], B. Pagare[57], P.R. Pais[22], T. Pajero[49], A. Palano[24], M. Palutan[28], G. Panshin[44], L. Paolucci[57], A. Papanestis[58,49], M. Pappagallo[24,i], L.L. Pappalardo[26,m], C. Pappenheimer[66], C. Parkes[63], B. Passalacqua[26,m], G. Passaleva[27], D. Passaro[35,t], A. Pastore[24], M. Patel[62], J. Patoc[64], C. Patrignani[25,k], A. Paul[69], C.J. Pawley[79], A. Pellegrino[38], J. Peng[5,7], M. Pepe Altarelli[28], S. Perazzini[25], D. Pereima[44], H. Pereira Da Costa[68], A. Pereiro Castro[47], P. Perret[11], A. Perro[49,13], K. Petridis[55], A. Petrolini[29,n], J.P. Pfaller[66], H. Pham[69], L. Pica[35,t], M. Piccini[34], L. Piccolo[32], B. Pietrzyk[10], G. Pietrzyk[14], D. Pinci[36], F. Pisani[49], M. Pizzichemi[31,49,p], V.M. Placinta[43], M. Plo Casasus[47], T. Poeschl[49], F. Polci[16,49], M. Poli Lener[28], A. Poluektov[13], N. Polukhina[44], I. Polyakov[44], E. Polycarpo[3], S. Ponce[49], D. Popov[7], S. Poslavskii[44], K. Prasanth[59], C. Prouve[47], D. Provenzano[32,l], V. Pugatch[53], G. Punzi[35,u], S. Qasim[51], Q. Qian[6], W. Qian[7], N. Qin[4,c], S. Qu[4,c], R. Quagliani[49], R.I. Rabadan Trejo[57], J.H. Rademacker[55], M. Ramírez García[83], M. Rama[35], V. Ramos De Oliveira[70], M. Ramos Pernas[57], M.S. Rangel[3], F. Ratnikov[44,44], G. Raven[39], M. Rebollo De Miguel[48], F. Redi[30,j], J. Reich[55], F. Reiss[63], Z. Ren[7], P.K. Resmi[64], R. Ribatti[50], G. Ricart[15,12], D. Riccardi[35,t], S. Ricciardi[58], K. Richardson[65], M. Richardson-Slipper[59], K. Rinnert[61], P. Robbe[14,49], G. Robertson[60], E. Rodrigues[61], E. Rodriguez Fernandez[47], J.A. Rodriguez Lopez[75], E. Rodriguez Rodriguez[47], J. Roensch[19], A. Rogachev[44], A. Rogovskiy[58], D.L. Rolf[49], P. Roloff[49], V. Romanovskiy[66], A. Romero Vidal[47], G. Romolini[26], F. Ronchetti[50], T. Rong[6], M. Rotondo[28], S.R. Roy[22], M.S. Rudolph[69], M. Ruiz Diaz[22], R.A. Ruiz Fernandez[47], J. Ruiz Vidal[82,aa], A. Ryzhikov[44], J. Ryzka[40], J.J. Saavedra-Arias[9], J.J. Saborido Silva[47], R. Sadek[15], N. Sagidova[44], D. Sahoo[77], N. Sahoo[54], B. Saitta[32,l], M. Salomoni[31,49,p], I. Sanderswood[48], R. Santacesaria[36], C. Santamarina Rios[47], M. Santimaria[28,49], L. Santoro[2], E. Santovetti[37], A. Saputi[26,49], D. Saranin[44], A. Sarnatskiy[78], G. Sarpis[59], M. Sarpis[63], C. Satriano[36,v], A. Satta[37], M. Saur[6], D. Savrina[44], H. Sazak[17], F. Sborzacchi[49,28], L.G. Scantlebury Smead[64], A. Scarabotto[19], S. Schael[17], S. Scherl[61], M. Schiller[60], H. Schindler[49], M. Schmelling[21], B. Schmidt[49], S. Schmitt[17], H. Schmitz[18], O. Schneider[50], A. Schopper[49], N. Schulte[19], S. Schulte[50], M.H. Schune[14], R. Schwemmer[49], G. Schwering[17], B. Sciascia[28], A. Sciuccati[49], S. Sellam[47], A. Semennikov[44], T. Senger[51], M. Senghi Soares[39], A. Sergi[29,n], N. Serra[51], L. Sestini[33], A. Seuthe[19], Y. Shang[6], D.M. Shangase[83], M. Shapkin[44], R.S. Sharma[69], I. Shchemerov[44], L. Shchutska[50], T. Shears[61], L. Shekhtman[44], Z. Shen[6], S. Sheng[5,7],

JHEP07(2026)071

V. Shevchenko[44], B. Shi[7], Q. Shi[7], Y. Shimizu[14], E. Shmanin[25], R. Shorkin[44], J.D. Shupperd[69], R. Silva Coutinho[69], G. Simi[33,r], S. Simone[24,i], N. Skidmore[57], T. Skwarnicki[69], M.W. Slater[54], J.C. Smallwood[64], E. Smith[65], K. Smith[68], M. Smith[62], A. Snoch[38], L. Soares Lavra[59], M.D. Sokoloff[66], F.J.P. Soler[60], A. Solomin[44,55], A. Solovev[44], I. Solovyev[44], N.S. Sommerfeld[18], R. Song[1], Y. Song[50], Y. Song[4,c], Y.S. Song[6], F.L. Souza De Almeida[69], B. Souza De Paula[3], E. Spadaro Norella[29,n], E. Spedicato[25], J.G. Speer[19], E. Spiridenkov[44], P. Spradlin[60], V. Sriskaran[49], F. Stagni[49], M. Stahl[49], S. Stahl[49], S. Stanislaus[64], E.N. Stein[49], O. Steinkamp[51], O. Stenyakin[44], H. Stevens[19], D. Strekalina[44], Y. Su[7], F. Suljik[64], J. Sun[32], L. Sun[74], D. Sundfeld[2], W. Sutcliffe[51], P.N. Swallow[54], K. Swientek[40], F. Swystun[56], A. Szabelski[42], T. Szumlak[40], S. T'Jampens[10], Y. Tan[4,c], M.D. Tat[64], A. Terentev[44], F. Terzuoli[35,49,x], F. Teubert[49], E. Thomas[49], D.J.D. Thompson[54], H. Tilquin[62], V. Tisserand[11], M. Tobin[5,49], L. Tomassetti[26,m], G. Tonani[30,49,o], X. Tong[6], D. Torres Machado[2], L. Toscano[19], D.Y. Tou[4,c], C. Trippl[46], G. Tuci[22], N. Tuning[38], L.H. Uecker[22], A. Ukleja[40], D.J. Unverzagt[22], E. Ursov[44], A. Usachov[39], A. Ustyuzhanin[44], U. Uwer[22], C. Vázquez Sierra[47], V. Vagnoni[25,49], V. Valcarce Cadenas[47], G. Valenti[25], N. Valls Canudas[49], H. Van Hecke[68], E. van Herwijnen[62], C.B. Van Hulse[47,z], R. Van Laak[50], M. van Veghel[38], G. Vasquez[51], R. Vazquez Gomez[45], P. Vazquez Regueiro[47], S. Vecchi[26], J.J. Velthuis[55], M. Veltri[27,y], A. Venkateswaran[50], M. Verdoglia[32], M. Vesterinen[57], D. Vico Benet[64], P. Vidrier Villalba[45], M. Vieites Diaz[49], X. Vilasis-Cardona[46], E. Vilella Figueras[61], A. Villa[25], P. Vincent[16], F.C. Volle[54], D. vom Bruch[13], N. Voropaev[44], K. Vos[79], G. Vouters[10], C. Vrahas[59], J. Wagner[19], J. Walsh[35], E.J. Walton[1,57], G. Wan[6], C. Wang[22], G. Wang[8], H. Wang[73], J. Wang[6], J. Wang[5], J. Wang[4,c], J. Wang[74], M. Wang[30], N.W. Wang[7], R. Wang[55], X. Wang[8], X. Wang[72], X.W. Wang[62], Y. Wang[6], Y.H. Wang[73], Z. Wang[14], Z. Wang[4,c], Z. Wang[30], J.A. Ward[57,1], M. Waterlaat[49], N.K. Watson[54], D. Websdale[62], Y. Wei[6], J. Wendel[81], B.D.C. Westhenry[55], C. White[56], M. Whitehead[60], E. Whiter[54], A.R. Wiederhold[63], D. Wiedner[19], G. Wilkinson[64], M.K. Wilkinson[66], M. Williams[65], M.J. Williams[49], M.R.J. Williams[59], R. Williams[56], Z. Williams[55], F.F. Wilson[58], M. Winn[12], W. Wislicki[42], M. Witek[41], L. Witola[22], G. Wormser[14], S.A. Wotton[56], H. Wu[69], J. Wu[8], Y. Wu[6], Z. Wu[7], K. Wyllie[49], S. Xian[72], Z. Xiang[5], Y. Xie[8], A. Xu[35], J. Xu[7], L. Xu[4,c], L. Xu[4,c], M. Xu[57], Z. Xu[49], Z. Xu[7], Z. Xu[5], D. Yang[4], K. Yang[62], S. Yang[7], X. Yang[6], Y. Yang[29,n], Z. Yang[6], Z. Yang[67], V. Yeroshenko[14], H. Yeung[63], H. Yin[8], X. Yin[7], C.Y. Yu[6], J. Yu[71], X. Yuan[5], Y Yuan[5,7], E. Zaffaroni[50], M. Zavertyaev[21], M. Zdybal[41], F. Zenesini[25,k], C. Zeng[5,7], M. Zeng[4,c], C. Zhang[6], D. Zhang[8], J. Zhang[7], L. Zhang[4,c], S. Zhang[64], S.L. Zhang[71], Y. Zhang[6], Y.Z. Zhang[4,c], Y. Zhao[22], A. Zharkova[44], A. Zhelezov[22], S.Z. Zheng[6], X.Z. Zheng[4,c], Y. Zheng[7], T. Zhou[6], X. Zhou[8], Y. Zhou[7], V. Zhovkovska[57], L.Z. Zhu[7], X. Zhu[4,c], X. Zhu[8], V. Zhukov[17], J. Zhuo[48], Q. Zou[5,7], D. Zuliani[33,r], G. Zunica[50]

[1] *School of Physics and Astronomy, Monash University, Melbourne, Australia*
[2] *Centro Brasileiro de Pesquisas Físicas (CBPF), Rio de Janeiro, Brazil*
[3] *Universidade Federal do Rio de Janeiro (UFRJ), Rio de Janeiro, Brazil*
[4] *Department of Engineering Physics, Tsinghua University, Beijing, China*
[5] *Institute Of High Energy Physics (IHEP), Beijing, China*

JHEP07(2026)071

[6] School of Physics State Key Laboratory of Nuclear Physics and Technology, Peking University, Beijing, China
[7] University of Chinese Academy of Sciences, Beijing, China
[8] Institute of Particle Physics, Central China Normal University, Wuhan, Hubei, China
[9] Consejo Nacional de Rectores (CONARE), San Jose, Costa Rica
[10] Université Savoie Mont Blanc, CNRS, IN2P3-LAPP, Annecy, France
[11] Université Clermont Auvergne, CNRS/IN2P3, LPC, Clermont-Ferrand, France
[12] Université Paris-Saclay, Centre d'Etudes de Saclay (CEA), IRFU, Gif-Sur-Yvette, France
[13] Aix Marseille Univ, CNRS/IN2P3, CPPM, Marseille, France
[14] Université Paris-Saclay, CNRS/IN2P3, IJCLab, Orsay, France
[15] Laboratoire Leprince-Ringuet, CNRS/IN2P3, Ecole Polytechnique, Institut Polytechnique de Paris, Palaiseau, France
[16] Laboratoire de Physique Nucléaire et de Hautes Énergies (LPNHE), Sorbonne Université, CNRS/IN2P3, Paris, France
[17] I. Physikalisches Institut, RWTH Aachen University, Aachen, Germany
[18] Universität Bonn - Helmholtz-Institut für Strahlen und Kernphysik, Bonn, Germany
[19] Fakultät Physik, Technische Universität Dortmund, Dortmund, Germany
[20] Physikalisches Institut, Albert-Ludwigs-Universität Freiburg, Freiburg, Germany
[21] Max-Planck-Institut für Kernphysik (MPIK), Heidelberg, Germany
[22] Physikalisches Institut, Ruprecht-Karls-Universität Heidelberg, Heidelberg, Germany
[23] School of Physics, University College Dublin, Dublin, Ireland
[24] INFN Sezione di Bari, Bari, Italy
[25] INFN Sezione di Bologna, Bologna, Italy
[26] INFN Sezione di Ferrara, Ferrara, Italy
[27] INFN Sezione di Firenze, Firenze, Italy
[28] INFN Laboratori Nazionali di Frascati, Frascati, Italy
[29] INFN Sezione di Genova, Genova, Italy
[30] INFN Sezione di Milano, Milano, Italy
[31] INFN Sezione di Milano-Bicocca, Milano, Italy
[32] INFN Sezione di Cagliari, Monserrato, Italy
[33] INFN Sezione di Padova, Padova, Italy
[34] INFN Sezione di Perugia, Perugia, Italy
[35] INFN Sezione di Pisa, Pisa, Italy
[36] INFN Sezione di Roma La Sapienza, Roma, Italy
[37] INFN Sezione di Roma Tor Vergata, Roma, Italy
[38] Nikhef National Institute for Subatomic Physics, Amsterdam, Netherlands
[39] Nikhef National Institute for Subatomic Physics and VU University Amsterdam, Amsterdam, Netherlands
[40] AGH - University of Krakow, Faculty of Physics and Applied Computer Science, Kraków, Poland
[41] Henryk Niewodniczanski Institute of Nuclear Physics Polish Academy of Sciences, Kraków, Poland
[42] National Center for Nuclear Research (NCBJ), Warsaw, Poland
[43] Horia Hulubei National Institute of Physics and Nuclear Engineering, Bucharest-Magurele, Romania
[44] Authors affiliated with an institute formerly covered by a cooperation agreement with CERN.
[45] ICCUB, Universitat de Barcelona, Barcelona, Spain
[46] La Salle, Universitat Ramon Llull, Barcelona, Spain
[47] Instituto Galego de Física de Altas Enerxías (IGFAE), Universidade de Santiago de Compostela, Santiago de Compostela, Spain
[48] Instituto de Fisica Corpuscular, Centro Mixto Universidad de Valencia - CSIC, Valencia, Spain
[49] European Organization for Nuclear Research (CERN), Geneva, Switzerland
[50] Institute of Physics, Ecole Polytechnique Fédérale de Lausanne (EPFL), Lausanne, Switzerland
[51] Physik-Institut, Universität Zürich, Zürich, Switzerland
[52] NSC Kharkiv Institute of Physics and Technology (NSC KIPT), Kharkiv, Ukraine
[53] Institute for Nuclear Research of the National Academy of Sciences (KINR), Kyiv, Ukraine
[54] School of Physics and Astronomy, University of Birmingham, Birmingham, United Kingdom

JHEP07(2026)071

[55] H.H. Wills Physics Laboratory, University of Bristol, Bristol, United Kingdom
[56] Cavendish Laboratory, University of Cambridge, Cambridge, United Kingdom
[57] Department of Physics, University of Warwick, Coventry, United Kingdom
[58] STFC Rutherford Appleton Laboratory, Didcot, United Kingdom
[59] School of Physics and Astronomy, University of Edinburgh, Edinburgh, United Kingdom
[60] School of Physics and Astronomy, University of Glasgow, Glasgow, United Kingdom
[61] Oliver Lodge Laboratory, University of Liverpool, Liverpool, United Kingdom
[62] Imperial College London, London, United Kingdom
[63] Department of Physics and Astronomy, University of Manchester, Manchester, United Kingdom
[64] Department of Physics, University of Oxford, Oxford, United Kingdom
[65] Massachusetts Institute of Technology, Cambridge, MA, United States
[66] University of Cincinnati, Cincinnati, OH, United States
[67] University of Maryland, College Park, MD, United States
[68] Los Alamos National Laboratory (LANL), Los Alamos, NM, United States
[69] Syracuse University, Syracuse, NY, United States
[70] Pontifícia Universidade Católica do Rio de Janeiro (PUC-Rio),[ab] Rio de Janeiro, Brazil
[71] School of Physics and Electronics,[ac] Hunan University, Changsha City, China
[72] State Key Laboratory of Nuclear Physics and Technology,[ad] South China Normal University, Guangzhou, China
[73] Lanzhou University,[ae] Lanzhou, China
[74] School of Physics and Technology,[af] Wuhan University, Wuhan, China
[75] Departamento de Fisica ,[ag] Universidad Nacional de Colombia, Bogota, Colombia
[76] Ruhr Universitaet Bochum,[ah] Fakultaet f. Physik und Astronomie, Bochum, Germany
[77] Eotvos Lorand University,[ai] Budapest, Hungary
[78] Van Swinderen Institute,[aj] University of Groningen, Groningen, Netherlands
[79] Universiteit Maastricht,[ak] Maastricht, Netherlands
[80] Tadeusz Kosciuszko Cracow University of Technology,[al] Cracow, Poland
[81] Universidade da Coruña,[am] A Coruña, Spain
[82] Department of Physics and Astronomy,[an] Uppsala University, Uppsala, Sweden
[83] University of Michigan,[ao] Ann Arbor, MI, United States

[a] Associated to: Universidade Estadual de Campinas (UNICAMP), Campinas, Brazil
[b] Associated to: Centro Federal de Educacão Tecnológica Celso Suckow da Fonseca, Rio De Janeiro, Brazil
[c] Associated to: Center for High Energy Physics, Tsinghua University, Beijing, China
[d] Associated to: Hangzhou Institute for Advanced Study, UCAS, Hangzhou, China
[e] Associated to: School of Physics and Electronics, Henan University , Kaifeng, China
[f] Associated to: LIP6, Sorbonne Université, Paris, France
[g] Associated to: Lamarr Institute for Machine Learning and Artificial Intelligence, Dortmund, Germany
[h] Associated to: Universidad Nacional Autónoma de Honduras, Tegucigalpa, Honduras
[i] Associated to: Università di Bari, Bari, Italy
[j] Associated to: Università di Bergamo, Bergamo, Italy
[k] Associated to: Università di Bologna, Bologna, Italy
[l] Associated to: Università di Cagliari, Cagliari, Italy
[m] Associated to: Università di Ferrara, Ferrara, Italy
[n] Associated to: Università di Genova, Genova, Italy
[o] Associated to: Università degli Studi di Milano, Milano, Italy
[p] Associated to: Università degli Studi di Milano-Bicocca, Milano, Italy
[q] Associated to: Università di Modena e Reggio Emilia, Modena, Italy
[r] Associated to: Università di Padova, Padova, Italy
[s] Associated to: Università di Perugia, Perugia, Italy
[t] Associated to: Scuola Normale Superiore, Pisa, Italy
[u] Associated to: Università di Pisa, Pisa, Italy
[v] Associated to: Università della Basilicata, Potenza, Italy

JHEP07(2026)071

[w] *Associated to: Università di Roma Tor Vergata, Roma, Italy*
[x] *Associated to: Università di Siena, Siena, Italy*
[y] *Associated to: Università di Urbino, Urbino, Italy*
[z] *Associated to: Universidad de Alcalá, Alcalá de Henares , Spain*
[aa] *Associated to: Department of Physics/Division of Particle Physics, Lund, Sweden*
[ab] *Associated to 3*
[ac] *Associated to 8*
[ad] *Associated to 4*
[ae] *Associated to 5*
[af] *Associated to 4*
[ag] *Associated to 16*
[ah] *Associated to 19*
[ai] *Associated to 49*
[aj] *Associated to 38*
[ak] *Associated to 38*
[al] *Associated to 41*
[am] *Associated to 46*
[an] *Associated to 60*
[ao] *Associated to 69*
[†] *Deceased*

JHEP07(2026)071